Carboxymethyl Cellulose, Functionalized Graphene Oxide based Ternary Composite for the Removal of Heavy Metal Lead (II): Batch and Column Studies

Gowri Gunasekaran[1], Daisy Rani James Durai[2], Neerazhagan Balaji Thimmarajampettai[3], Ali Zainul Abideen Ansar[4], Rekha Anantharaman[5] and Sudha Parappurath Narayanan[6]*

1. Department of Chemistry, DKM College for Women (Autonomous), Vellore, Tamil Nadu, INDIA
2. Department of Chemistry, SRM Institute of Science and Technology, Ramapuram Campus, Chennai, Tamil Nadu, INDIA
3. Department of Chemistry, PERI Institute of Technology, Mannivakkam, Chennai, Tamil Nadu, INDIA
4. Department of Chemistry, C Abdul Hakeem College (Autonomous), Melvisharam, Ranipet district, Tamil Nadu, INDIA
5. Department of Obstetrics and Gynecology, Saveetha Medical College and Hospital, Saveetha Institute of Medical and Technical Sciences (SIMATS), Chennai, Tamil Nadu, INDIA
6. Department of Physiology, Saveetha Dental College and Hospitals, Saveetha Institute of Medical and Technical Sciences (SIMATS), Saveetha University, Chennai, Tamil Nadu, INDIA

*drparsu8@gmail.com

Abstract

A functionalized graphene oxide (f-GO) based ternary composite was fabricated with carboxymethyl cellulose (CMC) and hydroxyapatite (HAp) and crosslinked with glutaraldehyde (GA) for the adsorptive removal of heavy metal lead (II) from water. The composite was characterized and the adsorption process was optimized through batch and column studies. Adsorption kinetics and mechanisms were investigated using adsorption isotherm studies. The results showed that the adsorption followed pseudo-second-order kinetics (R^2-0.9981) and the Freundlich isotherm (R^2-0.9965), indicating a heterogeneous surface and multilayer adsorption and pseudo-second-order kinetics.

The fixed bed column studies demonstrated that 1 cm of bed height, 200 mg/L of inlet concentration and 3 mL/min of flow rate were optimal for lead (II) removal. The functionalized graphene oxide based composite exhibited a high adsorption capacity and efficiency, making it a promising adsorbent for removing heavy metals from industrial effluent. The study highlights the potential of carboxymethyl cellulose, functionalized graphene oxide-based composites as an effective and eco-friendly solution for environmental heavy metal pollution.

Keywords: Carboxymethyl cellulose, f-GO, HAp, composite, lead removal.

Introduction

Due to their non-biodegradable nature, extreme toxicity even at low concentrations and widespread presence in food, drinking water, soil and air, heavy metal ions are a major cause of environmental pollution. Heavy metals are a major concern worldwide because of their toxicity, bioaccumulation and biomagnification in living organisms like plants and animals[96]. Heavy metals are among the most dangerous and enduring contaminants in industrial effluent[13]. Some of the polluting heavy metals are (Pb (II)), (As (III)), (Hg (II)), (Cr(VI)), (Cd (II)) found to be harmful and toxic[41] to the living ones even in trace amounts.

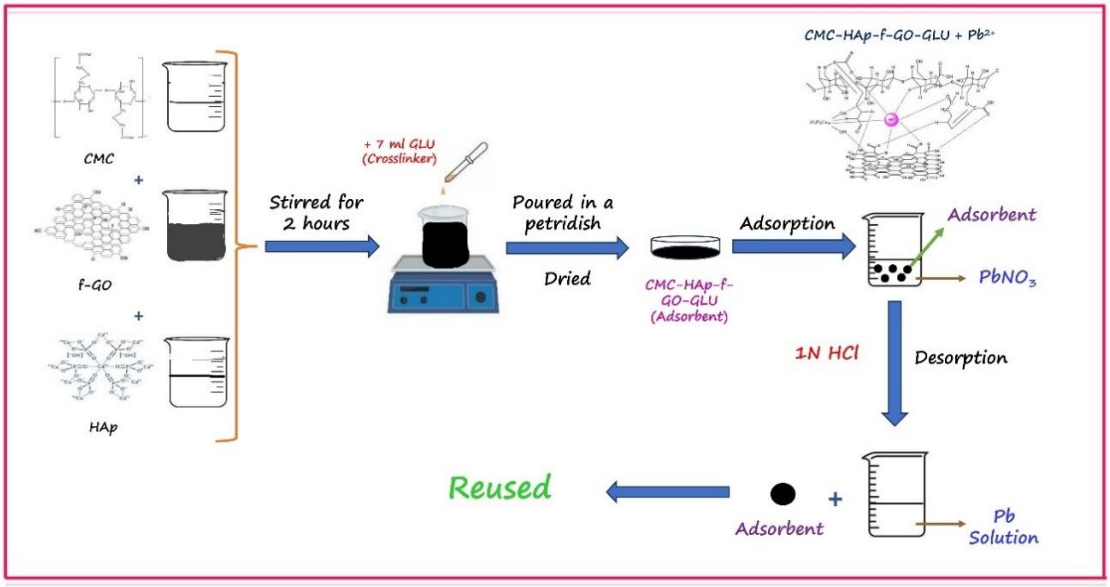

Graphical Abstract

The major use of lead is in making rechargeable storage batteries[6]. Lead is a highly poisonous metal that affects almost every organ in the body. The National Health and Nutrition Examination Survey (NHANES), USA, has calculated the level of lead(Pb) in blood in the U.S. populations of children whose elevated levels of blood lead were found to be (> 10µg/dL)[91]. The allowed level of lead in drinking water is 15 µg/L. Pb that is not biodegradable, can enter the food chain and severely compromises human physical fitness. Serious health issues that could arise from it include renal and lung disorders, semi-permanent brain stroke and cancer[25]. Lead poisoning shows a teratogenic effect[73]. Lead consumption damages the immune system, particularly the tissues in the kidneys. Human exposure to lead has been shown to have the following effects: mainly Alzheimer's disease and reduced fertility, both in men and women[55].

There have been reports of several methods, such as membrane separation, ion exchange, coagulation-precipitation and adsorption treatments that have been effective in eliminating heavy metals from industrial effluents[3]. However, these procedures are inefficient economically because they have inherent drawbacks over adsorption including inadequate dye removal, high energy needs, high running costs and the creation of by-products. Adsorption, on the other hand, is recognized as a prominent technique in this field due to its widespread use as a physicochemical technology. Many advantages of this approach include its simplicity of use, affordability, increased selectivity, higher efficiency, compatibility with the environment and ease of operation[62,69,75].

Given its benefits, including low secondary sludge production, cost-effectiveness and convenience of operation, one of the most promising methods for removing metals from wastewater is adsorption[35,90]. Thus, adsorption is a process primarily utilized in the water treatment sector and efforts have been made to identify inexpensive and efficient adsorbents[42].

Natural, biodegradable and reasonably priced polymers with a variety of functional groups including -NH_2, -COOH and -OH, such as polysaccharides, can be employed as adsorbents for heavy metal ions[17]. Modified polysaccharides are widely employed due to improved properties[60]. Most of the agricultural waste, cotton and wood pulp all naturally contain cellulose, a polysaccharide[50]. Due to the abundance of hydroxyl functional groups in cellulose, it can operate as a biopolymeric ligand. However, the adsorption capacity of cellulose may be greatly decreased because of the potential instability of the complexes that result from the interaction between the OH groups at positions C2 and C3 and the metal cations.

Carboxymethyl cellulose is a derivative of cellulosic material that has not yet been thoroughly studied or customized. According to Bao et al[11] and Hokkanen et al[27], carboxymethyl cellulose (CMC) is a cellulose derivative in which specific hydroxyl groups of the glucopyranose monomer ring that occupy the cellulose skeleton, are bonded with -CH_2-COOH groups. According to Rasoulzadeh and Namazi[67], as an anionic polymer, CMC has excellent film-forming properties, a high viscosity, resistance to oils, grease and organic solvents and quick dissolution in both hot and cold water.

In recent times, graphene oxide (GO) has garnered significant interest since it is an intriguing two-dimensional carbon-based substance having a high atomic thickness and specific surface area that has a high adsorption capacity. The functionalised graphene oxide is considered more attractive due to its higher functionality created by -COOH and -SO_3H and -OH groups. Thus, during the adsorption process, many hydroxyl and carboxyl groups on the GO surface supply a high number of active sites[26,44]. Accordingly, adding f-GO will enhance the adsorption capacity and dispersity of CMC in water[88]. According to Zhao et al[100], the removal of metal cations may also benefit from the use of the sulfonated magnetic GO composite.

Any polymer can be easily blended with graphene oxide to create a composite material that has better qualities than the original polymer such as thermal stability, mechanical strength and stiffness, electrical conductivity and tensile strength[81]. In the current work, a functionalization based on carboxyl group reinforcement into the graphene oxide matrix was carried out to improve the functional characteristics of graphene oxide.

The form and chemistry of hydroxyapatite (HAp), a calcium phosphate, are comparable to those of human hard tissues. The basic inorganic component of calcium apatite is hydroxyapatite, also known as hydroxylapatite[52]. Its formula is $Ca_5(PO_4)_3$, however, it is typically written $Ca_{10}(PO_4)_6(OH)_2$ to indicate that the crystal unit cell consists of two entities. Environmental researchers have recently considered this material because of its unique qualities which include extended shelf life, biocompatibility, biodegradability and a high specific surface area[20,30]. Several investigations have documented the appropriate operation of hydroxyapatite in processes such as calcium ion exchange with divalent metals/ions[80], immobilization[89] and adsorption[24].

Many crosslinkers including glutaraldehyde (GA), epichlorohydrin (EPC), tripolyphosphate (TPP), genipin and glyoxal, are frequently used to achieve chemical crosslinking[48,51]. Glutaraldehyde (GA) is one of the many crosslinkers that has been widely employed to create crosslinked, well-organized biopolymeric composites. Hence, in the present work, functionalized graphene oxide was fabricated with carboxymethyl cellulose and HAp with the crosslinking agent glutaraldehyde (GA) is employed in water as an adsorbent to extract lead (Pb) using batch adsorptive mechanisms. The applicability of the adsorption

process in the real-time situation was also tested by fixed-bed column studies. The study results are suitably tested using different isotherms and dynamic adsorption models.

Material and Methods

Materials: Hydroxyapatite was procured from Sigma-Aldrich Co. Graphite was obtained from Molychem Chemicals Ltd. Carboxymethyl cellulose, lead nitrate were procured from Riochem Chemical Pvt. Ltd. Glutaraldehyde was obtained from MPM scientific chemicals.

Synthesis of functionalized Graphene Oxide: GO was developed using graphite powder with a modification of Hummer's method[36]. One gram of graphite powder was dispersed in five mL of cold 98% sulfuric acid in an ice bath. 4 gms of $KMnO_4$ were gradually added within 5 min while stirring the liquid below 20°C, following 20 min of stirring. The reaction was kept continuing for 30 minutes at 35°C after one hour. Subsequently, 50 mL of deionized water was gradually added to the reaction blend. The solution was further diluted to 200 mL with deionized water after 20 min of reaction time at 98 °C. To eliminate any residual $KMnO_4$ and MnO_2, 5 mL of 30% H_2O_2 was added.

Subsequently, the end product underwent four rounds of continuous washing with 5% HCl solution and deionized water. The resulting f-GO (yield 89%) was vacuum-dried in an oven for ten hours at 70°C.

Preparation of carboxymethyl Cellulose/hydroxyapatite /f-graphene oxide composite: A minimum of one gram of carboxymethyl cellulose was dissolved in water. Simultaneously, 0.5 g of hydroxyapatite and 0.25 g of f-graphene oxide were dispersed in water. Each solution was thoroughly mixed using a magnetic stirrer for approximately 20 min. The stirred hydroxyapatite and functionalized graphene oxide solutions were slowly added to the carboxymethyl cellulose taken in a beaker. The resulting mixture was again magnetically stirred for about 2 hrs after the addition of 7ml of glutaraldehyde as the crosslinking agent and air dried in a Petri dish. The dried composite was subjected to various characterization studies.

Fourier Transform Infra-red Spectroscopy: The Shimadzu FT-IR Spectrometer, which has a range of 400–4000 cm^{-1}, was used to record the Fourier transform infrared spectrophotometer (FT-IR) spectrum.

X-ray Diffraction Analysis: The Ni filter Cu Kα radiation source (λ=0.154nm) was used to capture the X-ray diffraction pattern. The D8 advance diffractometer was operated with a voltage of 30 kV and a current of 40 mA.

Thermogravimetric Analysis: To investigate the weight losses at various phases, the SDT Q600 V8.0 Build 95 instrument was used in the TGA investigation. In a nitrogen environment, the instrument was heated at a rate of 10 °C per minute.

Differential Scanning Calorimetry: The Netzsch DSC 200 PC was used to conduct the measurements in an Al pan with a punctured lid, heating the material at a rate of 10 °C per minute in a N_2 atmosphere.

Scanning Electron Microscopy with EDX: Scanning electron microscopy was used to examine the composites' surface morphology to verify the compatibility of the polymers. For the analysis, using a sputter coater unit (VG – Microtech, UCK field, UK), a thin layer of gold-palladium was applied to the sample and the topography was studied with a JEOL Model JSM - 6390LV model and Oxford XMX N with a tungsten filament.

Antimicrobial Activity: The resultant composites' antibacterial effectiveness was evaluated in comparison to two Gram-negative and one Gram-positive bacterial strains namely *Staphylococcus aureus, Klebsiella pneumonia and Escherichia coli* utilizing the Muller Hinton agar (MHA) medium and the disc diffusion method, along with antifungal activity against *Aspergillus flavus*, *Aspergillus niger and Mucor* using Sabouraud dextrose agar in the present research work.

Antioxidant Activity: Antioxidants have a significant function in disease prevention. Hence in the present work, the antioxidant property of the composite was evaluated by the DPPH radical scavenging method.

DPPH Scavenging Activity: Using the DPPH scavenging experiment, the composite's antioxidant activity was investigated. The DPPH radical scavenging activity is an investigation of antioxidant capacity. The prepared composite's capacity to scavenge radicals was ascertained by measuring the absorbance of DPPH at 517nm. When the color changes, the sample scavenges the DPPH by donating hydrogen atoms to form a stable DPPH complex, which causes the absorbance to drop. DPPH solution without a sample is considered a control.

The following formula determined the percentage of inhibition (I%) of free radical generation from DPPH:

$$\%\ of\ inhibition\ = \frac{A_c - A_s}{A_c} * 100 \quad (1)$$

where Ac is Absorbance of the control and As is Absorbance of the sample solution.

Heavy metal lead removal using CMC/Hap/f-GO-GLU composite by batch adsorption: Lead nitrate solution with specified starting metal concentrations was used for batch investigations by using CMC/HAp/f-GO-GLU composite. The metal solution was taken in stoppered bottles and shaken in an orbital shaker at a constant speed of 210 rpm at 30 °C. The degree of metal removal was investigated separately by changing the parameters of pH, contact time, adsorbent dosage and starting metal ion concentration. The heavy

metals' adsorption was analyzed using Varian AAA 220 FS Atomic Absorption Spectroscopy after each treatment stage.

An analysis was conducted on the lead adsorption process under optimal pH, duration of contact, dose of adsorbent and initial concentration of metal ions. Both Freundlich and Langmuir isotherms were fitted to the data. The formula for the Langmuir equation is:

$$\frac{C_{eq}}{C_{ads}} = \frac{bC_{eq}}{K_L} + \frac{1}{K_L} \quad (2)$$

$$C_{max} = \frac{K_L}{b} \quad (3)$$

where C_{ads} is the metal ion adsorbed quantity (mg/g), C_{eq} is the metal ion's equilibrium concentration in solution (mg/dm^3). The Langmuir constant, or K_L, is represented in dm^3/g. b = Langmuir constant (dm^3/mg).

The highest amount of metal ions that can bind to an adsorbent is expressed as C_{max} (mg/g). The Freundlich equation used is expressed as:

$$C_{ads} = K{C_{eq}}^{1/n} \quad (4)$$

The Freundlich equation was expressed in a linearized form.

$$logC_{ads} = \log K + 1/n \log C_{eq} \quad (5)$$

where C_{ads} are the amount of metal ions adsorbed (mg/g), Freundlich constant (mg/g-1) is represented by 1/n and C_{eq} is the equilibrium concentration in solution (mg/dm^3) and K = Freundlich contant (g.dm^{-3}).

By conducting a different set of adsorption experiments at constant temperatures to track the adsorption over time, the adsorption process's kinetics could be studied. Using the pseudo-first- and pseudo-second-order models, it is possible to determine quantitatively and evaluate the adsorption rate.

Pseudo first-order equation:

$$\log(q_e - q_t) = logq_e - k_1 t/2.303 \quad (6)$$

Pseudo Second-order equation:

$$t/q_t = 1/k_2\, q^2 e + t/q_e \quad (7)$$

The adsorption rate constants of pseudo-first order and pseudo-second order kinetics are represented by the expressions qe and qt respectively and K_1 (min^{-1}) and K_2 (g mg^{-1} min^{-1}) are the amounts of metal adsorbed (mg/g) at equilibrium at time t (min). The pseudo-first-order and pseudo-second-order models are represented in the linear charts by tracing log (qe - qt) versus t and (t/qt) versus t respectively. The visualization of the experimental data yields the rate constants k_1 and k_2.

Intraparticle diffusion Kinetics: The equation for intraparticle diffusion is expressed as follows:

$$q_t = K_{id} t^{1/2} + C \quad (8)$$

where K_{id} is the intraparticle diffusion rate constant (mg/g min$^{1/2}$) and C is the intercept. Plotting q_t vs t $^{1/2}$ allowed for getting K_{id} and C values based on the slope and intercept.

Desorption Studies: A desorption study was also carried out for the lead-loaded composites after the adsorption process was over. Desorption studies were done using 1N HCl as the desorbing agent. 0.5 g of the lead-loaded adsorbent was weighed and treated with 1N HCl, shaken well for 2 hours and filtered. Then, the lead concentration in the filtrate was analyzed using AAS studies.

Column Adsorption Studies: For the experiment, a Pyrex glass tube with an inner diameter of 2.1 cm and a height of 30 cm served as the fixed bed column. Lead nitrate was used to study the removal efficiency of the adsorbent through the column. The metal solution was supplied to the column with a downward flow. At regular intervals, a filtered sample was gathered. The heavy metal lead was analyzed after each period of remediation using an Atomic Absorption spectrometer. Three dynamic models: the Boharts and Adam, Thomas and Yoon Nelson models as well as breakthrough curves, were used during the continuous adsorption process that varied the impact of flow rates.

Thomas Model: The linearised form of the Thomas model for an adsorption column was expressed as follows:

$$ln\frac{C_0}{C_t} - 1 = \frac{K_{TH} q_0 X}{Q} - \frac{K_{TH} C_o}{Q} V_{eff} \quad (9)$$

where C_t and C_o are the concentrations of inlet and effluent solutes (mg/L), The formula for calculating the maximum adsorption capacity is q_o (mg/g), the total mass of the adsorbent is X (g), the inlet volumetric flow rate is Q (mL/min), the throughput volume is V_{eff} (mL); and the Thomas rate constant is k_{TH} = mL/min.mg. The equilibrium absorption per gram of the adsorbent and q_o can be found by analyzing the slope and intercept of the plot of ln (C_o/C_t)-1 against throughput volume (V_{eff}). The kinetic coefficient is k_{TH}.

Yoon Nelson Model: The linear form of the Yoon and Nelson model is represented as follows:

$$\ln\left[\frac{C_t}{C_0 - C_t}\right] = K_{YN} t - \tau K_{YN} \quad (10)$$

where t is the breakthrough (sampling) time (min), τ is the time needed for 50% adsorbate breakthrough (min), C_t and C_o are the effluent and inlet solute concentrations and k_{YN} is the Yoon and Nelson rate constant (min^{-1}). With the help of the slope and intercept of the plot of ln (C_o-C_t) versus t, the k_{YN} and τ values were calculated.

Adam Bohart Model: The Adam-Bohart expression is provided as follows:

$$\ln\left[\frac{C_t}{C_0}-1\right]=\frac{K_{AB}C_0tZ}{F}-K_{AB}N_0 \quad (11)$$

where Z is the column bed depth (cm), F is the superficial velocity of the influent solution determined by dividing the flow rate by the column section area (cm/min) and C_t and C_o are the effluent and influent concentrations (mg L^{-1}) at time t and zero and k_{AB} is the kinetic constant (mL/min.mg). The parameters (k_{AB} and N_o), which characterize the characteristic operations of the column, were found using the slope and intercept of the plot of ln (C_t /C_o) against time (t) respectively.

Results and Discussion

In the present work, carboxymethyl cellulose (CMC), hydroxyapatite (HAp) and carboxyl functionalized graphene oxide crosslinked with glutaraldehyde (1:0.5:0.25 + 7 ml glutaraldehyde) were prepared and characterized by FT-IR, XRD, TGA, DSC, SEM, antimicrobial and antioxidant techniques. Subsequently, batch adsorption studies determined the prepared CMC/HAP/f-GO-GLU composite's adsorption capacity. Removal of heavy metal lead required adjusting variables like starting metal ion concentration, pH, adsorbent dose and contact time. The results of the characterizations and various parameters were carried out for the adsorption process:

Fourier Transform Infrared spectroscopy: Information regarding the existence or lack of particular functional groups and the identification of crosslinked networks present in the composites are best provided by FT-IR. The FT-IR spectrum of the CMC/HAp/f-GO composite made using the cross-linking material glutaraldehyde is given in figure 1. The FT-IR spectrum of the crosslinked CMC/HAp/f-GO-GLU composite shows prominent and distinctive peaks that represent each of the polymeric matrix's groups involved in the crosslinked composite formation. The broadband that appears at 3427.51 cm^{-1} involves carboxymethyl cellulose's O-H stretching vibration overlapping with the O-H stretching of HAp and f-GO due to an intermolecularly H-bonded O-H stretched vibration that has raised vibration transferred to an area with a higher wavenumber as a result of the crosslinking that occurred[84,99].

The absorption peaks at 2929.87 cm^{-1} and 2358.94 cm^{-1} are assigned to the asymmetric C-H stretching in methylenic and C=O stretching in O=C=O anhydride moiety[98]. The appearance of C=O asymmetric stretching vibration gives a strong peak at 1633.71 cm^{-1} due to the carboxylate group. A strong peak observed at 1716.65 cm^{-1} indicates the presence of C=O stretching vibration of aldehydic linkages, confirming the formation of glutaraldehyde cross linked composite[40].

The development of a new peak at 1116.78 cm^{-1} corresponds to the C-O-C and C-O stretch in ethers and alcohol groups present in the CMC and GO overlapping during composite formation with glutaraldehyde. A small peak obtained at 1346.31 cm^{-1} indicates the O-H bending and C-H symmetrical deformation vibration of CMC. A 1051.20 cm^{-1} sharp peak indicates C-O stretching vibration in alcohol, C-O-C and P-O asymmetric stretching vibrations[31,48,72,101]. This overlap of O-H and P-O stretching vibrations confirms the presence of HAp and f-GO, which are included in the CMC matrix. The PO_4^{3-} - bending mode of HAp was confirmed by the presence of a peak at 565.14 cm^{-1}. Certain peaks at 781.17 cm^{-1} and 617.22 cm^{-1} refer to the C-H bending and O-H out-of-plane bending in CMC[21,63].

The above-observed peaks for the crosslinked composite confirmed the involvement of strong hydrogen bonding among the CMC, HAp and f-GO with the crosslinker glutaraldehyde due to the appearance of two peaks at 1716.65 cm^{-1} and 1346.31 cm^{-1} which are indicative of the interaction between them and glutaraldehyde, a physical crosslinking agent that encourages hydrogen bonded interactions in polymers and improves the polymers' miscibility[53].

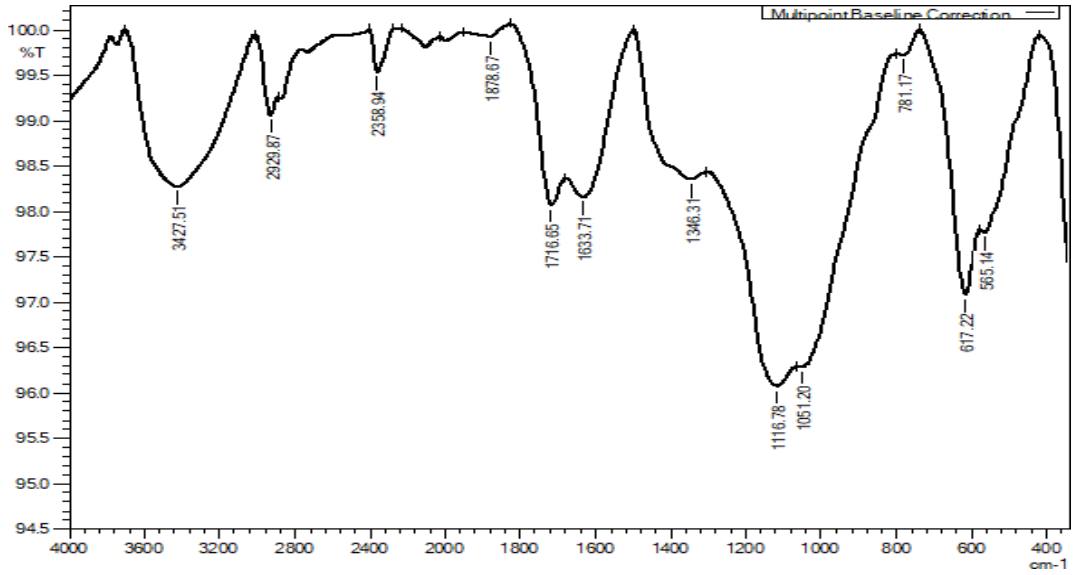

Figure 1: FT-IR spectrum of CMC/HAp/f-GO-GLU composite

X-ray diffraction analysis: One common technique for characterizing various polymeric materials for the investigation of atomic spacing and crystal structures is X-ray diffraction (XRD). XRD is most often employed in measuring the crystallinity in polymers. The constructive interference of a crystalline sample with monochromatic X-rays is the fundamental process of X-ray diffraction. The identification of unknown crystalline materials such as minerals and inorganic compounds, is the most popular use of X-ray powder diffraction. The X-ray diffractogram details of the CMC/HAp/f-GO-GLU crosslinked composite are shown below. Figure 2 and Table 1 represent the composite's percentage of crystallinity.

The X-ray diffractogram of the glutaraldehyde crosslinked composite is shown in figure 2. The XRD pattern of the composite exhibits a 2θ shift to 25° on comparing it with the composite prepared without crosslinker (22°). This shift in the diffraction peak was due to the addition of the crosslinking agent glutaraldehyde. In addition, 8.4% was determined as the percentage of the degree of crystallinity. The degree of crystallinity was found to be reduced by the addition of the crosslinker. It can be seen that the apatite peaks observed at 31.39°, 32.4° and 33.53° are consistent with the standard XRD peaks of the HAp[8].

This pattern also includes the characteristic and new peaks at 26° and 39° when compared to Hap, which were attributed to f-GO being well dispersed with the HAp and CMC matrix[45,87]. This reduction in the range of diffraction peaks of the crosslinked composite shows the interaction between the polymers through hydrogen bonding upon the addition of the crosslinker glutaraldehyde. The reduction in the percentage of the degree of crystallinity reveals that the CMC/HAp/f-GO-GLU composite is highly amorphous which highly favors the adsorption process[74].

Thermogravimetric analysis (TGA): Thermogravimetry (TGA) is the method that uses a thermogravimetric analyzer (TGA) or thermobalance to measure a sample's mass versus temperature or time. This is a helpful tool to study the volatile quantities, decomposition profile, thermal and oxidative stability of the sample under analysis. The TGA thermogram of the crosslinked CMC/HAp/f-GO-GLU composite is shown in the figure 3. The TGA thermogram of the crosslinked CMC/HAp/f-GO-GLU composite shows that decomposition of the sample occurs at three stages of weight loss. The first stage reveals the evaporation of water molecules and moisture up to 250 °C with a small weight loss of a sample of 7.4%[1].

A major weight loss of up to 36.9 % starting from 300 °C – 590 °C has taken place, which indicates that the thermal degradation of the carbon skeleton present in f-GO is due to the destruction of carboxyl, hydroxyl and epoxy groups of GO[92,95]. This increase in the decomposition of the sample was attributed to the crosslinking that had taken place effectively, which increased the thermal stability of the sample. Upon completion of the experiment, after fast degradation up to 500 °C, there is a least significant decomposition, indicating the higher thermal stability of the composite noticed at 790 °C degradation temperature, which may be possibly due to the decomposition of HAp dispersion in the composite. The crosslinker glutaraldehyde enhanced the thermal stability of HAp. After subtraction of weight loss, it was estimated that when the experiment was over, around 44.6% of the material was still in residue, showing the high thermal stability of the composite[64,79].

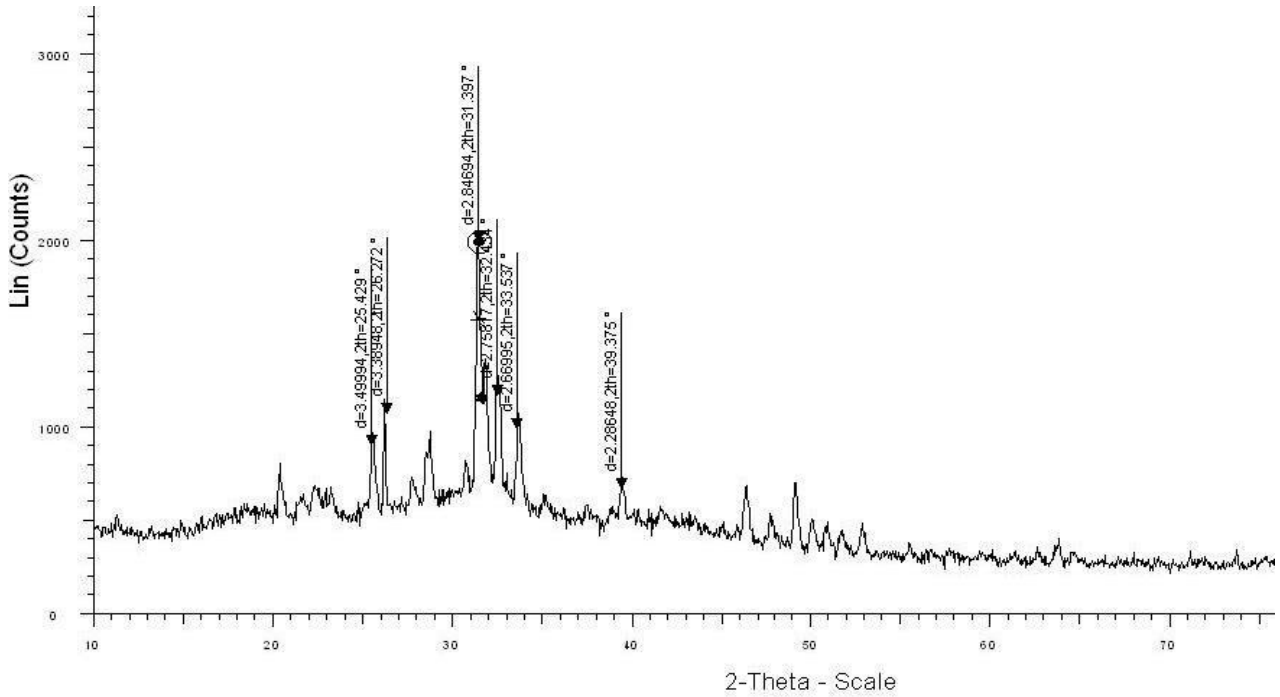

Figure 2: X-ray diffractogram of CMC/HAp/f-GO-GLU composite
(X-ray diffraction details of CMC/HAp/f-GO-GLU composite)

Table 1
X-ray diffraction details of CMC/HAp/f-GO-GLU composite

Sample	2θ values	Degree of crystallinity (%)
CMC/HAp/f-GO (Unpublished work)	22°, 26°, 32°, 33°, 34° and 40°	15.5
CMC/HAp/f-GO-GLU	25°, 26°, 31°, 32°, 33° and 39°	8.4

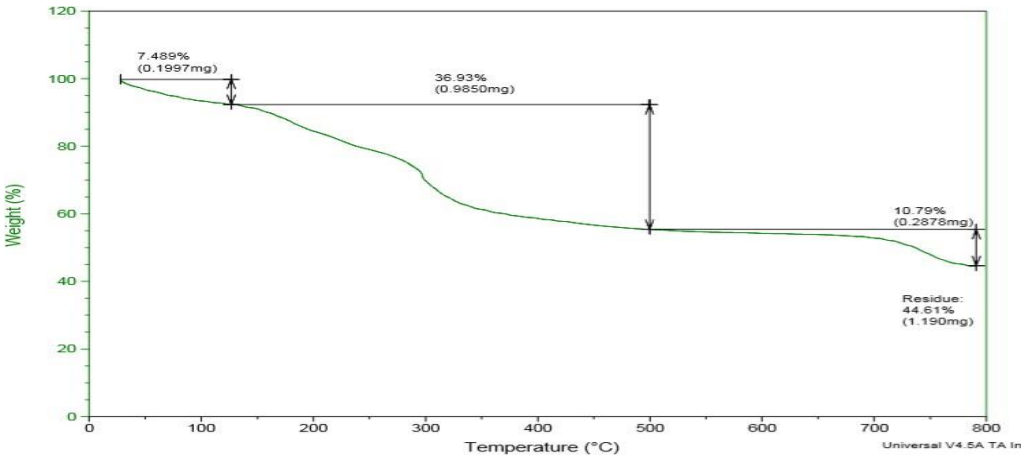

Figure 3: TGA thermogram of CMC/HAp/f-GO-GLU composite

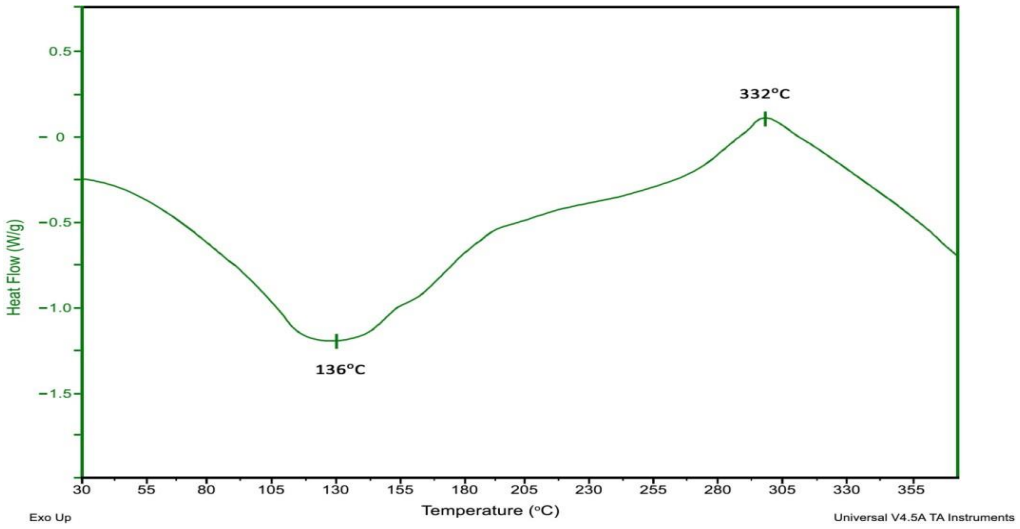

Figure 4: DSC thermogram of CMC/HAp/f-GO-GLU composite

Differential scanning calorimetric analysis (DSC): DSC analysis is a thermoanalytical tool to monitor how materials behave with temperature. When a sample is heated, cooled, or maintained isothermally at a constant temperature, the heat flow developed in the sample is measured using DSC analysis[16]. The glass transition temperature, crystalline phase transition temperature and decomposition or melting temperature are measured using DSC analysis. The CMC/HAp/f-GO-GLU composite's DSC thermogram is shown in figure 4. The cross-linked CMC/HAp/f-GO-GLU composite's DSC thermogram displays a broad, wide endothermic peak at 136°C which is caused by the sample's absorbed water molecules evaporation. At this point, crystallization starts to take place.

The composite's enhanced thermal stability is indicated by the single glass transition temperature of 230°C. The higher is the glass transition temperature, greater is the stability of the sample. The composite's decomposition temperature is suggested by the exothermic peak which appears at 332°C. On comparing the crosslinked CMC/HAp/f-GO-GLU composite with the uncrosslinked one, due to its higher glass transition temperature of 230°C than the composite made without glutaraldehyde, which has a glass transition temperature of 204°C (Unpublished work), the former was shown to be more thermally stable. On account of the comparison, glutaraldehyde crosslinked composite shows higher melting temperature because of the high fusion of the crosslinker with the composite, providing thermal resistance to the sample[93].

Scanning electron microscopy studies (SEM): With a

Scanning electron microscope (SEM), one can obtain three-dimensional polymer morphology and topography by measuring the particle size, shape and texture of the substance in milligram quantities only. It is cost-effective and inexpensive to operate. It is a surface characterization technique used to obtain quantitative data of the sample image related to size and shape distribution over the sample's surface. The SEM micrograph details of the CMC/HAp/f-GO-GLU composite are represented in figure 5.

The morphology of the glutaraldehyde cross-linked composite did show micro and macro pores in the 50 µm and 100 µm magnification range. The deposition of the CMC surface with HAp and f-GO particles caused the composite to become highly porous and irregular. The composite has a highly rough texture with good interconnectivity between the pore walls, provided mainly by the crosslinker, which favors the adsorption process[28]. This uniform distribution of irregular pores with a pore size of 7.3 µm makes the composite superadsorbent[33]. This pore size is responsible for providing active and binding sites for the adsorbent to be essential to the metal ions' adsorption[46]. From the evidence of the rough and porous texture, which improves the removal of metal ions, it can be decided that the developed composite will be a more promising adsorbent for the adsorption process.

Antimicrobial Activity: Since the fouling of the adsorbents has an impact on adsorption when continuously used, the antimicrobial properties will help to prevent them from fouling easily. Hence the efficiency of the glutaraldehyde crosslinked CMC/HAp/f-GO composite was tested against bacterial species such as *Proteus mirabilis*, *Escherichia coli* also known as *E. coli and Staphylococcus aureus*, the fungal species like *Aspergillus flavus, Aspergillus niger and Mucor sp.* using well diffusion method.

Antibacterial activity: The antibacterial activity of the CMC/HAp/f-GO-GLU composite was tested against Gram-negative bacterial species like *Proteus mirabilis* and *E. coli* and Gram-positive species *Staphylococcus aureus*. The zone of inhibition value of the prepared composite was measured in mm against the chosen bacteria's growth. The developed composite's antibacterial activity screening impact against the chosen bacterial species is shown in the table 2.

a) Antifungal activity: The antifungal activity of CMC/HAp/f-GO-GLU composite was tested against *Aspergillus flavus, Aspergillus niger and Mucor sp.* by well diffusion method. The CMC/HAp/f-GO-GLU composite's zone of inhibition values against the growth of the chosen fungi are expressed in millimeters. The findings of the screening for antifungal activity of the CMC/HAp/f-GO-GLU composite are listed in table 3.

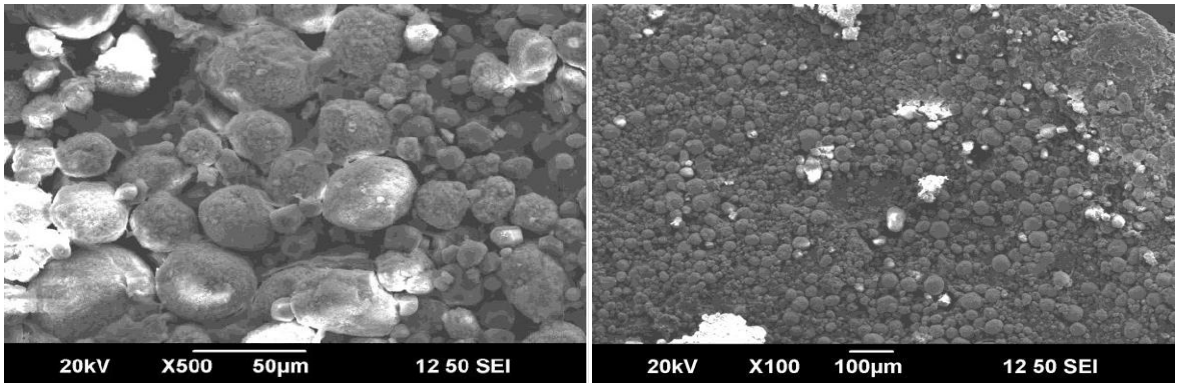

Figure 5: Surface morphology images of CMC/HAp/f-GO-GLU composite

Table 2
Antibacterial activity data of the CMC/HAp/f-GO-GLU composite againstbacterial species measured in mm

Organism	Diameter of Zone of Inhibitionin mm CMC/HAp/f-GO-GLU composite (mm)	Control (Ampicillin) (mm)
E.coli	27	12
Proteus mirabilis	25	15
Staphylococcus aureus	29	18

Table 3
Antifungal activity data of the CMC/HAp/f-GO-GLU composite against fungal species measured in mm

Organism	Diameter of Zone of Inhibition in mm CMC/HAp/f-GO-GLU composite	Diameter of Zone of Inhibition in mm Control (Polymyxin Bsulfate)
Aspergillus flavus	31	12
Aspergillus niger	28	15
Mucor sp.	30	18

The developed composite's zone of inhibition values against bacterial and fungal species indicate a higher bacteriocidal and fungicidal effect on the tested bacterial and fungal species. The composite shows an antibacterial effect on *E.coli* and *staphylococcus* than *proteus* with the zone of inhibition value in mm around 27 mm, 29 mm and 25 mm respectively. Higher fungicidal activity on *Aspergillus flavus* and *Mucor sp.* rather than *Aspergillus niger* with the zone of inhibition value 31 mm, 30 mm and 28 mm respectively was recorded. It can be noted that the glutaraldehyde crosslinked composite was found to have a higher antibacterial and fungal activity which may be explained because of the increased functional surface.

The bacteriocidal and bacteriostatic effect of the graphene-based materials showed physical damage to the bacterial membrane and caused bacterial death[43]. The wrapping of the graphene oxide sheet induces membrane stress[4]. The primary mechanisms of bacterial inactivation are reactive oxygen species-induced oxidative stress (ROS) and damage to cell membranes from coming into close contact with graphene oxide's sharp edges. Graphene-based materials with HAp show a bacteriostatic effect through favorable affinity for bacterial adhesion[76]. Graphene oxide-based materials, binding upon treatment with crosslinking agents, still further enhance the bacteriocidal effect on the microorganisms[29].

Therefore, it can be said that cross-linked composite is a potential source appropriate for biomedical applications and has outstanding antibacterial and antifungal properties and materials present in the polymeric matrix to protect the adsorbent from bacterial and fungal attacks[49].

Antioxidant activity: Carboxymethyl cellulose is a linear polysaccharide[77]. Hydrophilic properties of CMC may restrict their everyday usage, but they can be overcome by combining with other biopolymers to recover their usage with low cost and appropriate mechanical features[19]. Crosslinking agents are the best way to increase the hydrophobicity and mechanical properties to render CMC for various applications[57]. The scavenging activity of the glutaraldehyde crosslinked CMC/HAp/f-GO composite was tested by using the 2,2-diphenyl-1-picrylhydrazyl (DPPH) method. The antioxidant activity of the glutaraldehyde crosslinked CMC/HAp/f-GO composite was tested by the DPPH method by taking various concentrations of the composite. Figure 6 illustrates that the scavenging activity of the prepared composite shows an increase in antioxidant activity of the composite with the increase in the concentration of the composite, such as 10 mg/ml to 60mg/ml.

Enzymatic and non-enzymatic antioxidant defenses are how antioxidants keep the process by which free radicals are created[34]. Chemicals called antioxidants aid in decreasing or stopping the harm that free radicals can do. The reactive oxygen species present in the CMC, combined with functionalized graphene oxide, act as scavengers that may protect cells against the effects of free radicals. Incorporating glutaraldehyde into the polymer matrix significantly increases the antioxidant activity of the other polymers[22]. Hence, it can be concluded that the composite has good and higher antioxidant activity against the free radical generation.

Batch Adsorption Studies: The unfavorable consequence of heavy metal pollution poses a significant risk to human survival and the discharge of these heavy metals in wastewater has increased in the last three decades[14]. The pre-treatment required to remove these heavy metals before contaminating the environment involves the adsorption process. The wide availability of carbon resources in the various forms of their composites[58] due to their properties with two-dimensional nature makes them applicable to remove contaminants[71]. The primary goal of this project is to examine the adsorption capacity of theCMC/HAp/f-GO-GLU composite to extract lead (II) metal from wastewater. The developed composite's adsorption capacity was evaluated and the adsorption process's progress was monitored continuously by optimizing the various parameters. The results of the optimized parameters are discussed.

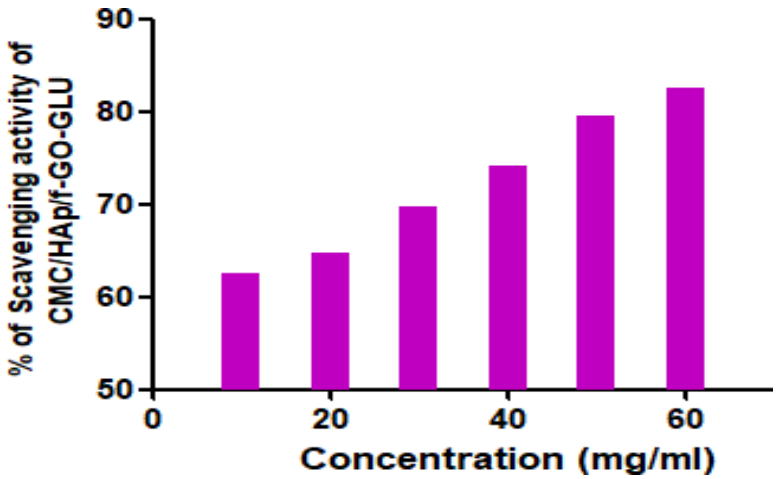

Figure 6: Antioxidant scavenging activity of the CMC/HAp/f-GO-GLU composite

Effect of pH: The impact of pH on Pb (II) removal via adsorption in aqueous solution onto the CMC/HAp/f-GO-GLU composite is shown in figure 7. By changing the metal ion solution's pH, the crosslinked composite's adsorption capacity was examined from 4 to 9 for lead metal by keeping other parameters constant. The adsorption increases when the metal solution's pH reaches pH 6, according to the results of the pH effect shown in figure 7. The higher is the pH value, the lower is the adsorption capability. For Pb (II), a pH of six was optimum with 82.75% removal.

The amount of metal ions removed decreases at lower pH levels because of the presence of strongly protonated H^+ and H_3O+ ions that cover the biosorbents' surface and also stop metal ions from adhering to the adsorbents, reducing the amount of heavy metals that are absorbed[68]. Since GO maintains a stronger electrostatic interaction between the positively charged adsorbate metal solution and the negatively charged adsorbent surface, the presence of metal ions was shown to decrease as pH increased[73]. Further raising the pH of the solution causes metal hydroxides to develop, which strongly repel using electrostatic interactions. The GO surface contains negatively charged oxygenous functional groups that lower the adsorption capability[94].

Effect of adsorbent dose: The effect of the dose of adsorbent on the CMC/HAp/f-GO-GLU composite's adsorptive removal of Pb (II) is shown in figure 8. Based on the dosage of the adsorbent, the percentage of metal ion removal was assessed by changing the amount of adsorbent from 0.5 g to 2.5 g while maintaining a pH of 6 and agitating the mixture for 1 hour at a concentration of 100 mg/L of metal ions.

Figure 8 shows that when the dosage of adsorbent is raised (i.e. from 87.52% to 89.88%), the elimination of metal ions is also reduced. The initial rise in the adsorption process was caused by a greater proportion of binding sites for the metal ions with the adsorbent up to 2g. As time goes on, the concentration of the metal ions decreases, rendering the adsorbent dose ineffective[97]. When a high sorbent dose is employed, the adsorbent has more accessible active sites than metal ions do. This results in a minor increase in adsorbent saturation at the lowest possible concentration of adsorbate[23].

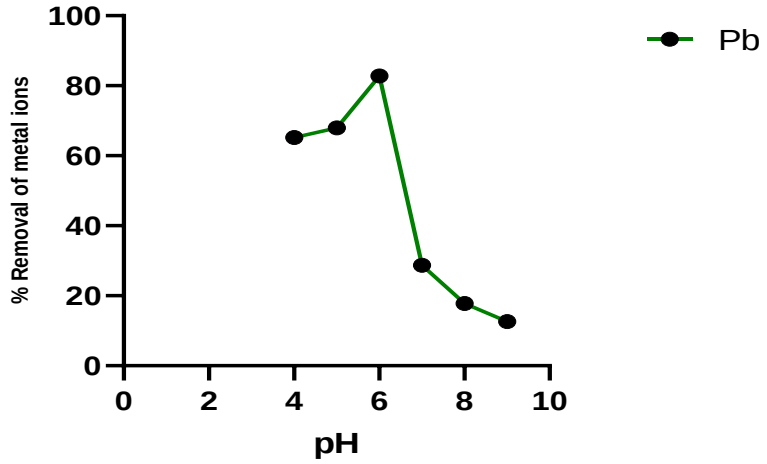

Figure 7: Impact of pH on Pb (II) ion removal from aqueous solution utilizing CMC/HAp/f-GO-GLU composite

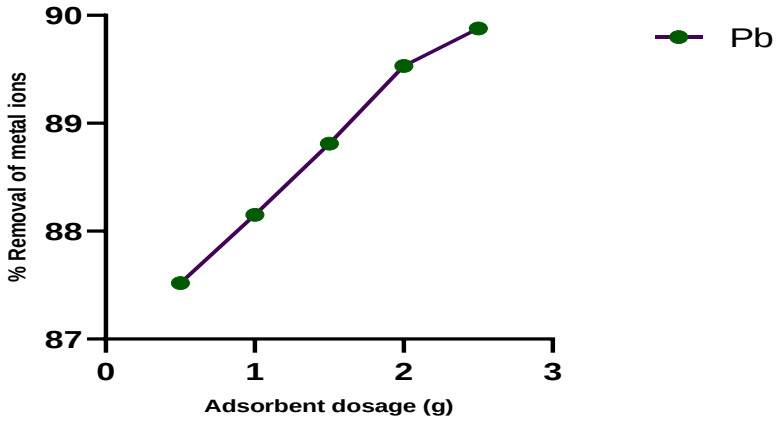

Figure 8: The effect of adsorbent dosage on Pb (II) ion removal from aqueous solution utilizing CMC/HAp/f-GO-GLU composite

Effect of contact time: Figure 9 illustrates the effect of changing the contact period from 30 minutes to 180 minutes on Pb (II) adsorption on the composite CMC/HAp/f-GO-GLU. The optimum conditions for the progress of the contact time involve a constant pH of 6. The agitation time was 1h, keeping the constant metal ion concentration at 100 mg/L.

When contact duration increases, so does the removal percentage of Pb (II) ions, from 77.99% to 94.74% (from 30 min to 180 minutes), as illustrated in figure 9. It is noteworthy that after 120 minutes, there is no appreciable rise in adsorption. After the number of metal ions has occupied all of the adsorbent's active sites, the second stage entails reaching equilibrium. The percentage of metal ion removal rises as the contact duration increases because more accessible adsorbent active sites are occupied by the metal ions[52]. This creates constancy in the removal percentage without any significant change due to the complete saturation of the adsorbent sites at 120 minutes. The active sorbent surface containing the target metal ions is the cause of the rise in removal percentage[85].

Effect of starting concentration of metal ions: The impact of the starting metal content is a critical component in predicting how well the adsorption process will remove heavy metals. By adjusting the metal ion concentration from 500 mg/L to 31.25 mg/L, the effect of the concentration of metal ions on the CMC/HAp/f-GO-GLU composite was studied. Figure 10 shows the effect of the initial metal ion concentration on the adsorption of Pb (II) onto CMC/HAp/f-GO-GLU composite with a constant pH 6 for Pb and an agitation time of 1h with the adsorbent dose 0.5g for all the concentrations.

Adsorption isotherms: Adsorption is typically described by the association between the activity or equilibrium concentration of the adsorbent and the amount of adsorbate that adheres to the surface at a constant temperature is expressed by the adsorption isotherm. In other words, adsorption isotherms depict how an adsorbent and an adsorbate interact. The graphical representation of isotherms involves a plot showing the adsorbate quantities adsorbed on the adsorbent surface at a constant temperature. Adsorption isotherms provide much more detail about the adsorption process. They reveal whether or not the adsorbate and adsorbent have an attractiveinteraction[61].

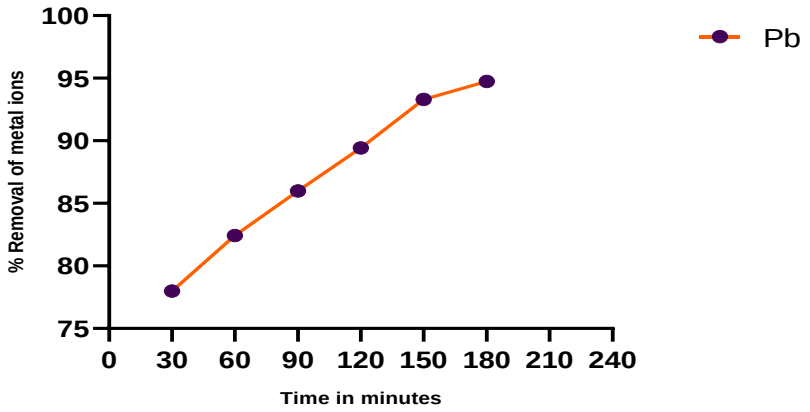

Figure 9: Impact of contact duration on Pb (II) heavy metal removal from aqueous solution using CMC/HAp/f-GO-GLU composite

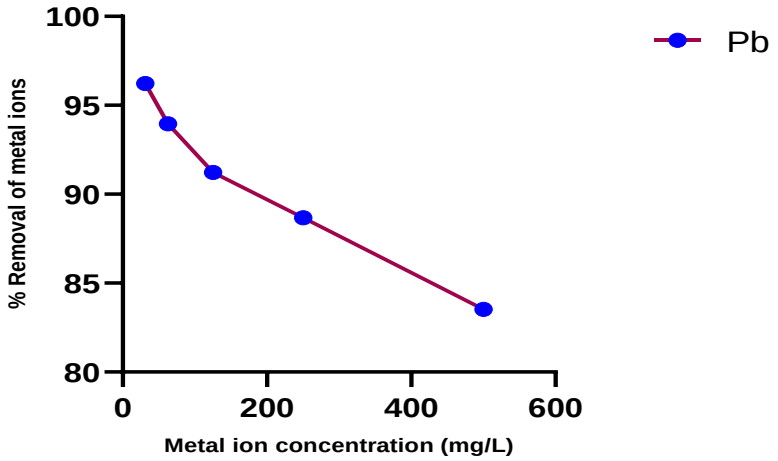

Figure 10: Effect of starting concentration on the removal of Pb (II) ions

Langmuir and Freundlich adsorption isotherm models: At adsorption equilibrium, the adsorption process optimization is explained by various adsorption models. The prominent and most helpful methods for predicting the adsorption isotherms are (i) Langmuir and (ii) Freundlich which are used in the present work to describe the equilibrium coefficients and the adsorbent's ability to remove lead from an aqueous solution onto a cross-linked CMC/HAp/f-GO-GLU composite.

After applying the Langmuir adsorption isotherm equation to the results, the Langmuir constants KL and b were found using the slope and intercept of the linear plot of the Ceq/Cads vs Ceq[18]. Plotting of the Langmuir adsorption isotherms for Pb (II) adsorption ontoCMC/HAp/f-GO-GLU composite is represented in figure 11a. Freundlich adsorption isotherm model mainly applies to heterogeneous surfaces by assuming multilayer adsorption[80]. This linear plot of log q_e vs log C_e can be used to calculate the exponential coefficient 1/n and the Freundlich isotherm constant K_F. The linear regression coefficient plot for Pb (II) adsorption on the surface of the CMC/HAp/f- GO-GLU composite is depicted in figure 11b.

The computed values of the Langmuir adsorption isotherm constants are shown in table 5 which indicates that the C_{max} value for lead was 64.45 mg/g. The calculated correlation coefficient value (R^2) was 0.8289 for lead metal. Table 4 also represents the calculation value for the Freundlich adsorption isotherm constant parameters K_f = 2.5380 for Pb (II) metal ions and the value of n lies between 1-10, indicating that significant adsorption has taken place in the very low concentration of the adsorbent. When 1/n is smaller than 1, it shows that the adsorbent's capability for adsorption governs the adsorption in the way of the chemisorption process. The 1/n values predict the character of the process of adsorption by the conditional factors to determine whether the isotherm is favorable (0<1/n<1), irreversible (1/n = 0), or unfavorable (1/n>1). The above-mentioned computed findings showed a suitable adsorption process for removing metal ions which is found to be (0<1/n<1)[10].

The correlation coefficient (R^2) for Pb (II) metal was found to be greater for the Freundlich adsorption isotherm, ie. 0.9965, as compared to the Langmuir isotherm model (0.8289), according to a comparison of the expected values of the Langmuir and Freundlich isotherm constants for the isotherms, thus proving that effective multilayer adsorption has occurred on the adsorbent's surface[86]. However, both models were in good agreement in terms of predicting the adsorption process's progress. Heavy metals are typically adsorbed on adsorbents through electrostatic, hydrophobic, chelation, ion exchange, hydrogen bonding, precipitation, reduction, complexation, π-π, or weak Van der Waals interactions to name a few mechanisms[72]. One, two, or more of these interactions, alone or in combination, drive the adsorption process forward. Hence, a combination of electrostatic interaction, van der Waals force and complexation may be the type of interactions expected between the -OH groups and -COO^- of the CMC, Hap, f-GO and Lead ions.

Kinetics of adsorption: Investigating kinetic models facilitated the determination of the adsorption process's reaction rate and mechanism under ideal conditions to predict the suitable model capable of explaining the reaction process. Higher adsorption capacity and a quicker adsorption process rate are characteristics of an effective adsorbent[9]. Three different adsorption kinetic models including intra-particle diffusion, pseudo-first-order and pseudo-second-order models, were utilized in this investigation (Figures 12a, b and c) to examine the experimental data.

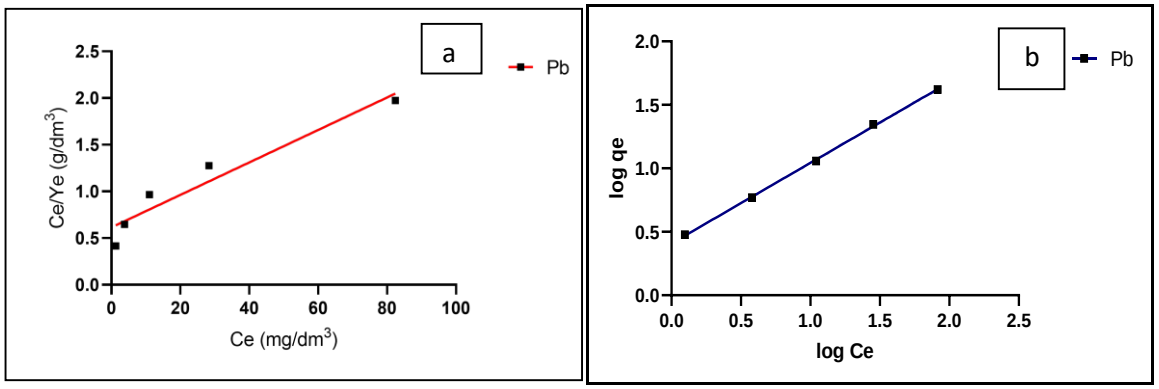

Figure 11: a) Langmuir adsorption isotherm b) Freundlich adsorption isotherm plots for lead (II) onto CMC/HAp/f-GO-GLU composite

Table 4
Langmuir and Freundlich constants for Pb (II) removal onto CMC/HAp/f-GO composite

Metal ions	Langmuir constants				Freundlich constant		
	K_L (dm^3/g)	b (dm^3/mg)	C_{max} (mg/g)	R^2	K_f	N	R^2
Pb (II)	1.6113	0.0250	64.45	0.8289	2.5380	1.5228	0.9965

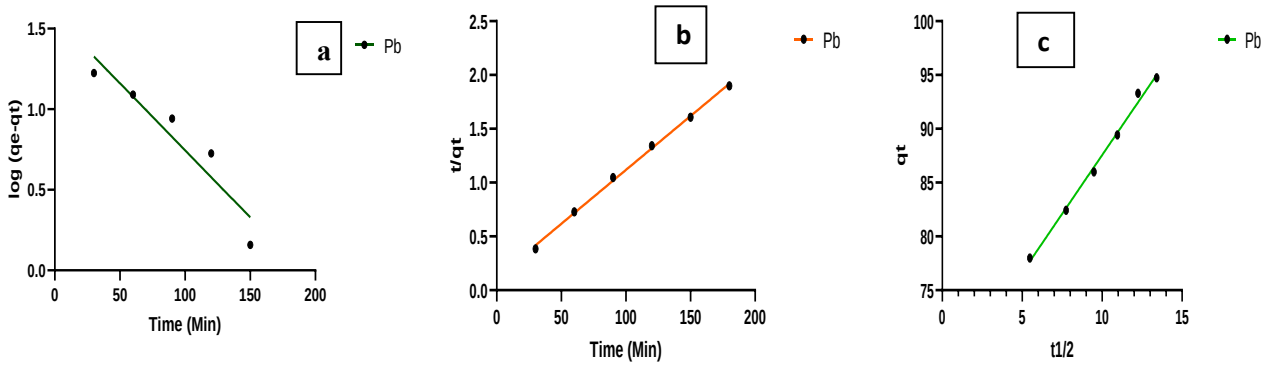

Figure 12: a) Pseudo-first-order b) Pseudo-second-order c) Intraparticle diffusion kinetic plot of Pb (II) onto CMC/HAp/f-GO-GLU composite

Table 5
Comparison of intra-particle diffusion models and Lagergren pseudo-first and pseudo-second order kinetics for Lead (II) adsorption by CMC/HAp/f-GO-GLU Composite

Metal	Pseudo-first-order kineticmodel			Intra particle diffusion			Pseudo-second-order kineticmodel		
	q_e (mg/g)	k_1 (min^{-1})	R^2	K_d	I	R^2	q_e (mg/g)	k_2 (g mg^{-1} min^{-1})	R^2
Pb (II)	75.51	0.0192	0.8930	4.368	131.4	0.9944	199.8	0.000428	0.9981

Pseudo-first-order (PSO) and Pseudo-second-order kinetics: The first-order rate constant, k_1 is obtained from the slope of the log (q_e–q_t) against the time plot. The kinetic plot of the pseudo-first-order for the Pb (II) onto the CMC/HAp/f-GO- GLU composite is shown in figure 12a. The pseudo-second-order kinetic plot for the Pb (II) onto the CMC/HAp/f-GO composite is shown in figure 12b.

Intraparticle diffusion: The mechanism of the adsorption process is understood by using the intraparticle diffusion model, an adsorption model that describes the diffusion of metal ions through the macro and micro pores of the adsorbent. Diffusion mechanisms involving pores, films and intraparticles are included in this model. This model's linearized form is expressed as follows:

$$qt = kid\ t^{1/2} + C$$

where the slope of the linear plot of q_t versus $t^{1/2}$ can be used to find the intraparticle diffusion rate constant (mg/g $min^{1/2}$) and C is the intercept. As the intercept increases, so will the boundary layer effect. The graphs illustrating intraparticle diffusion of Pb (II) onto CMC/HAp/f-GO-GLU composite are shown in figure 12c. For the intraparticle diffusion model, pseudo-first-order and pseudo-second-order correlation coefficients and rate constants are computed and are represented in table 5.

The tabulated kinetics of the adsorption process are explained by correlation coefficients R^2 equal to or near 1 or relatively high R^2 values of the anticipated models in table 5. The plots of log (qe-qt) Vs t for pseudo-first-order, qt Vs $t^{1/2}$ for the intraparticle diffusion model and the plot of t/qt Vs t for the pseudo-second-order model were plotted and their R^2 values were compared. The linear and straight line that passes through the origin with the higher correlation coefficient of R^2 = 0.9981 for Pb (II) ions was then discovered to be provided by the pseudo-second-order kinetic model. In addition, there is also a deviation in the linear plot and reduced pseudo-first-order diffusion and intraparticle correlation coefficient (R^2) values.

In contrast to pseudo-first-order and intraparticle diffusion models, the removal of metal ions Lead (II) in the adsorption process by CMC/HAp/f-GO-GLU composite was carried out according to the pseudo-second-order kinetic model based on the obtained data. The aforementioned data led to the conclusion that Pb (II) ion adsorption onto CMC/HAp/f-GO-GLU composite involves a chemical reaction between the electron transitions of the adsorbent and adsorbate and is modeled by a pseudo-second-order kinetic model.

The aforementioned data led to the conclusion that Pb (II) ion adsorption onto CMC/HAp/f-GO-GLU composite involves a chemical reaction between the electron transitions of the adsorbent and adsorbate and is modeled by a pseudo-second-order kinetic model. The square of the adsorbent's vacant site count determines how many active sites are occupied. The confirmation of metal ion uptake onto cross-linked CMC/HAp/f-GO-GLU composite was done by analyzing the metal-loaded composite by FT-IR spectrum for both thePb (II) metal-loaded composites. The details of the FT-IR spectrum are represented in the figure 13.

The FT-IR spectral details of the Pb (II) loaded CMC/HAp/f-GO-GLU composite show that a broad peak appeared at 3435.22 cm^{-1} and 3427.51cm^{-1} corresponding to the O-H stretching vibration due to the intermolecular hydrogen

bonding[47]. The appearance of C=O asymmetric stretching vibration gives a strong peak at 1633.71 cm^{-1} in the case of unadsorbed composite which shifted to 1627.92 cm^{-1} for both the Pb (II) loaded composite due to the carboxylate group in cases of metal loaded composite.

The development of a new peak at 1747.51 cm^{-1} for Pb (II) adsorbed composite with reduced intensity indicates that the cross-linking agent glutaraldehyde is involved in the coordination with the composite and also in chelation with the metal ion in which this peak is absent in the case of without crosslinked composite[66]. Certain peaks observed at 1392.61 cm^{-1} and 1400.32 $cm^{-1,}$ due to C-O stretching of carboxylate ion group and –OH bending, were identified by the shift from 1346.31 cm^{-1} In the absence of metal loading, the composite confirms the inclusion and contribution of carboxylic groups to the removal process.

The peak's disappearance at 1116.78 cm^{-1} and the appearance of a sharp and single intense peak observed at 1039.63 cm^{-1} for Pb (II) metal-loaded composite was the shift from 1051.20 cm^{-1} corresponding to P-O asymmetric stretching, indicating that these groups support the metal ion chelation towards the composite. The major shift of characteristic peak for the –OH group from 3427.51 cm^{-1} to 3435.22 cm^{-1} in the metal metal-loaded composite illustrates the attachment of metal by the hydroxyl groups of the composite effectively[37].

In addition, mainly metal-carbon, metal-nitrogen and metal-oxygen bonding will be observed in the case of the metal ion adsorption process. The peaks that were noted at 565.14 cm^{-1} and 617.22 cm^{-1} for the CMC/HAp/f-GO-GLU composite were shrunk into a single sharp and strong peak at 588.29 cm^{-1} for the lead-loaded composite during the metal chelation process. Therefore, based on the data above, it may be claimed that carboxyl and hydroxyl groups, along with the phosphate group in the composite, are helpful in the removal process to take place effectively. It proved to be an efficient adsorbent. Based on the evidence of the FT-IR spectrum taken after the adsorption of Pb (II) metal, the mechanism is proposed for the metal ion attachment to the active sites of the CMC/HAp/f-GO-GLU adsorbent as in figure 14.

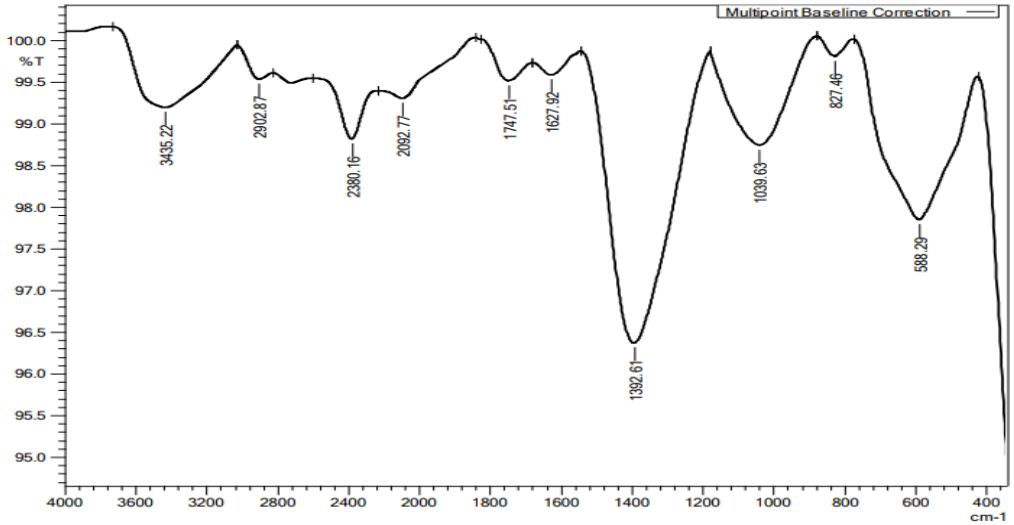

Figure 13: FT-IR spectrum of CMC/HAp/f-GO-GLU composite after adsorption of Pb (II) heavy metal

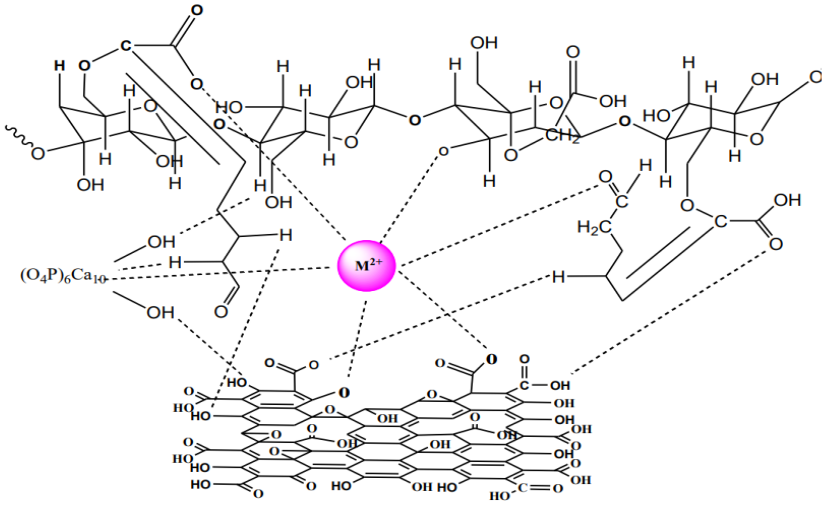

Figure 14: Binding mechanism for the metal ion onto CMC/HAp/f-GO-GLUcomposite

Energy Dispersive Scanning Electron Micrographic Analysis (EDX-SEM): The confirmation of the metal ions' adsorption onto the surface of the CMC/HAp/f-GO-GLU composite has been done by another technique, namely EDX spectral analysis. The EDX spectral analysis details for the Pb (II) metal-loaded CMC/HAp/f-GO-GLU composite are given in figure 15. The attachment of Pb (II) metal ions to the composite's surface was demonstrated by the EDX study conducted the metal ion adsorption process. Initially, the presence of some calcium ions in the hydroxyapatite was replaced by the lead metal during the adsorption process and the appearance of more characteristic peaks for carbon, oxygen and metal ion peaks showed the effective adsorption of heavy metal removal process by the glutaraldehyde cross-linked composite taking part in chelation of metal ions[65].

Desorption process: It is critical to test the adsorbent's reversibility after the adsorption process has been shown through the desorption process. To reduce the consequences of adsorbents that exist in wastewater by producing toxicity to the environment, investigation on the regeneration and reusability of the adsorbents has been done through desorption studies[70]. Here we have taken HCl as the desorbing agent, which is found to be more effective and faster for desorbing Pb^{2+} from the CMC/HAp/f-GO-GLU adsorbent. Following the completion of the adsorption process, 0.5g of the metal-loaded adsorbent was added to 50 ml of 0.1N HCl as the desorbing agent and the desorbing process was done by the cycle of time intervals of 30 min, 60 min, 90 min and 120 min.

The above results (Figure 16), based on the sequence of consecutive cycles, indicate that the ion exchange mechanism is responsible for Pb (II) desorption from the adsorbent, with a percentage of 98.90% for lead in the first step of the consecutive cycle. At the end of the experiment, it remains constant with a contact time of 2 h in the desorption process. Hence, the reusability and regeneration of the composite have been proved by the desorption process. Batch adsorption studies provide the efficacy or capacity of the adsorbent to remove impurities. However, the interaction time is insufficient for real-time process applications. Modeling the column test is important for predicting the adsorbent's large-scale adsorption behavior and utilizing it practically.

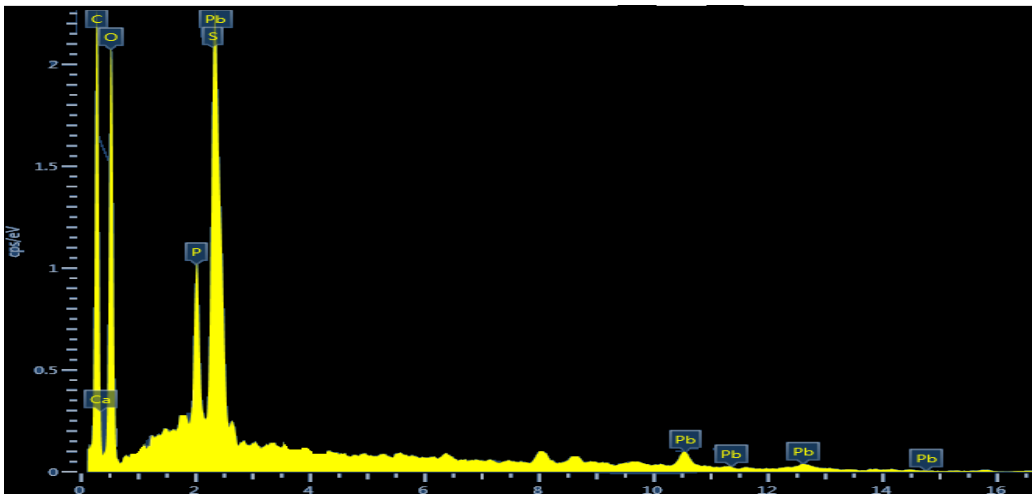

Figure 15: EDX of Lead loaded CMC/HAp/f-GO-GLUcomposite

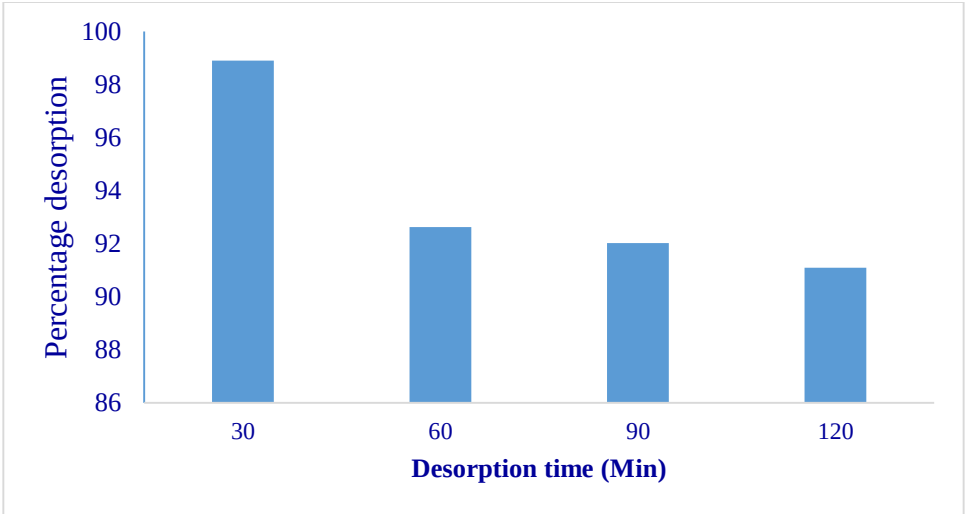

Figure 16: Desorption process by 0.1N HCl on metal-loaded CMC/HAp/f-GO-GLUadsorbent

Hence, continuous column studies are appropriate to study the hazardous heavy metal removal from fixed-bed columns. Column operation is the main method by which an assessment is made of a sorbent's practical value in removing impurities from wastewater[5]. For this reason, the dynamic column adsorption investigations were done in the present study to determine the composite system's practical applicability.

Column Studies: Column adsorption is monitored through the eluent's solute concentration over time or as a function of the volume going out of the column. It is possible to alter the solute concentration, flow rate and bed height. The adsorption process in a fixed-bed column depends on both time and distance. The breakthrough curves can be used to describe the column's efficiency. Plotting column effluent concentration vs treated volume or treatment time provides a breakthrough curve[102]. Within a static bed column adsorption system, several factors that influence the performance of continuous biosorption, including in packed bed reactors, the flow rate in volume and the starting concentration of metal ions, have been studied. Three optimization cycles have been completed to maintain a consistent bed height of 1 cm, as well as the potential for recycling and column regeneration.

Effect of flow rate: In the current investigation, by altering the flow rate of the solution, the impact of flow rate was assessed within a range of 1.0 mL/min to 3.0 mL/min while keeping the starting metal ion concentration of 200 mg/L and the bed height at 1.0 cm constant. The breakthrough curve, Ct/Co versus time under different flow rate treatments with a fixed bed depth of 1.0 cm and metal ion concentration of 200 mg/L is shown in figure 17 for Pb (II) adsorption onto CMC-HAp-f-GO-GLU composite. When compared to the greater flow rate (3.0 mL/min), the column performed well at the reduced rate of flow (1.0 mL/min), as evidenced by the breakthrough curve obtained for the flow rate plotted above which also shows a longer breakthrough time and longer saturation time.

A reduction in volumetric flow rate from 3.0 to 1.0 mL/min proved more advantageous ion exchange/adsorption conditions. This can be the result of the prolonged residence duration of the metal ions on the adsorbent, which lengthens the time it takes for the metal ions to diffuse into the adsorbent's pores via intraparticle diffusion[78]. Because equilibrium is reached faster at greater flow rates, the breakthrough curves get steeper and achieve the breakthrough sooner[38]. Hence, at a 200 mg/L metal ion concentration, 1.0 cm constant bed height and a flow rate of 1.0 mL/min, the produced adsorbent CMC-HAp-f-GO-GLU exhibits a greater adsorption capacity. This is consistent with the results that have been reported by Taty-Costodes et al[83].

Effect of initial metal ion concentration: A continuous flow technique was used to examine the Pb (II) ion concentration at the start of the adsorption process. The concentration ranged from 100 mg/L to 300 mg/L, with a bed height of 1 cm and a flow rate of 3.0 mL/min. The breakthrough curves on the CMC-HAp-f-GO-GLU composite at different starting metal ion concentrations are represented in figure 18. It is evident that as the starting metal ion concentration increased, so did the efficiency of removal, the breakthrough time and the residence time of columns. Because of the slow movement of metal ions onto the CMC-HAp-f-GO-GLU composite, breakthroughs occurred slowly and breakthrough curves appeared at reduced amounts of influent metal ions. The presence of enough active sites for the metal ions to be adsorbed may be the cause of the higher removal efficiency at lower metal ion concentrations. The percentage of metal ions removed decreases at greater metal ion concentrations because there are comparatively more metal ions than adsorption sites available[7].

Column Adsorption capacity and removal efficiency: The adsorption results for various metal ion concentrations, flow rates and constant bed heights are summarized in table 6. The obtained values represented in table 6 indicate that the ideal flow rate and initial concentration of metal ions for the removal of Pb (II) onto CMC/HAp/f-GO-GLU composite are therefore determined by the fact that, with an initial metal ion concentration of 100 mg/L, the percentage removal of metal ions was determined to be 3 mL/min at constant bed height of 1 cm. This percentage decreases with an increase in flow rate and metal ion concentration at constant bed height.

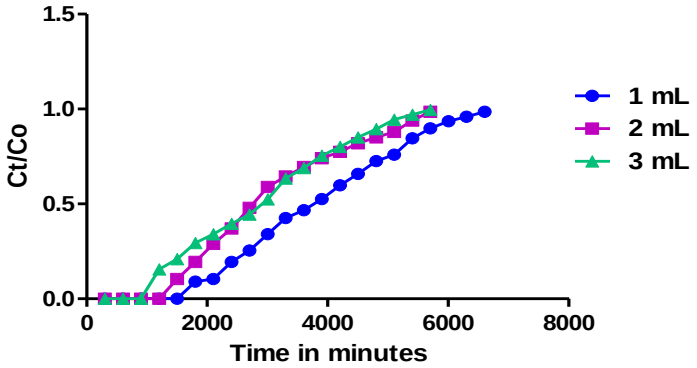

Figure 17: Effect of various flow rates on the breakthrough curve of Pb (II) adsorption onto CMC-HAp-f-GO-GLU composite

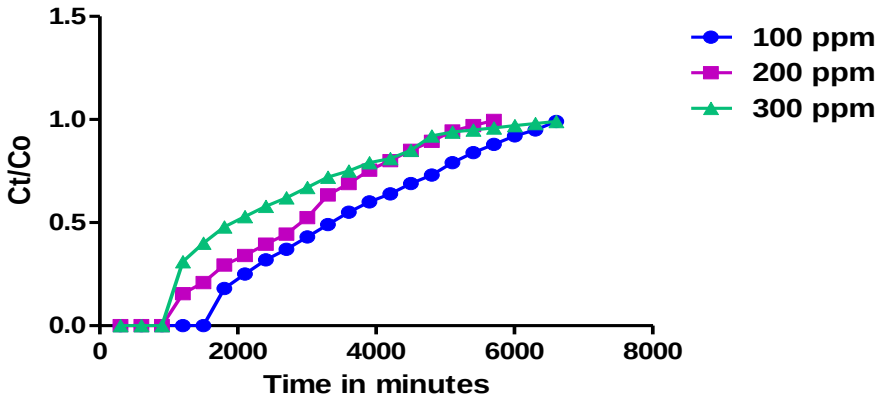

Figure 18: Effect of various initial metal ion concentrations on the breakthrough curve of Pb (II) adsorption onto CMC-HAp-f-GO-GLU composite

Table 6
Adsorption data obtained at constant bed heights and various flow rates and metal ion concentration

Metal ion	Flow Rate(Q) (mL/min)	Bed height (Cm)	Initial metal ion concentration (C_o) (mg/L)	Break through time (t_b) (min)	Saturation Time (t_{total}) (min)	q total (mg)	m total (mg)	Total removal (%)
Pb(II)	**Effect of Flow Rate**							
	1	1	200	1800	6600	816	1140	71.58
	2	1	200	1500	5700	1156.8	2280	50.74
	3	1	200	1200	5700	1192	2280	47.89
	Effect of Initial Metal Ion Concentration							
	3	1	100	1800	6600	993.3	1140	87.13
	3	1	200	1500	5700	1192	2280	47.89
	3	1	300	1200	5700	1298.3	2280	30.82

Column breakthrough kinetic modelling: The successful outcome is that for the adsorbate to adsorb, the fixed bed column technique depends on the adsorbent's adsorption capability. which is very important for the adsorption system and also for the prediction of various parameters involved in column operations which becomes significant under operating conditions[59]. For this purpose, several mathematical models such as Adam Bohart, Wolborska, Thomas, Clark, Yoon Nelson, Dose-Response and Bed Depth Service Time (BDST) models have been developed for the evaluation of efficiency and column models' suitability for large-scale operations[82]. Three popular models: the Yoon-Nelson model, the Adams-Bohart model and the Thomas model, were utilized to assess column performance achieved for flow rate and starting metal ion concentration, as well as to determine breakthrough curves in the present study.

Adam Bohart model: In the Adams-Bohart model, the adsorption rate is thought to be proportional to the solid's residual capacity as well as the concentration of the adsorbing species[12]. The Adam-Bohart model describes the first portion of the breakthrough curve. This model states that the rate of sorption is proportionate to the fraction of sorption capacity and that the equilibrium is not attained quickly[39].

The Adam-Bohart expression is given as:

$$\ln\left(\frac{C_o}{C_t}\right) = K_{AB}N_0\frac{Z}{F} - K_{AB}C_0t$$

where F is the linear flow rate (L min^{-1}), t is the duration (min), Z is the column's bed depth (cm) and N_0 is the saturation concentration (mg L^{-1}) and the concentrations of the influent and effluent are C_t and C_o (mg L^{-1}). The intercept and slope of a linear plot of ln (C_t/C_o) against time (t) were used to define the parameters describing the typical operations of the column (k_{AB} and N_0).

Figure 19 represents the Adam Bohart model's linear plot of experimental data at varying flow speed, starting metal ion concentrations and constant bed height for CMC-HAp-f-GO-GLU composite on lead (II) adsorption. Table 7 represents the values of the correlation coefficients and Adam Bohart model parameters that were determined using the analysis of linear regression under different conditions for the CMC-HAp-f-GO-GLU composite on lead (II) adsorption.

Plotting ln(C_t/C_o) against t (time) at a fixed bed height (z) and flow rate (F) allows for the evaluation of K_{AB} and N_0. where N_0 is the adsorption capacity and K_{AB} is the Adams-Bohart rate constant.

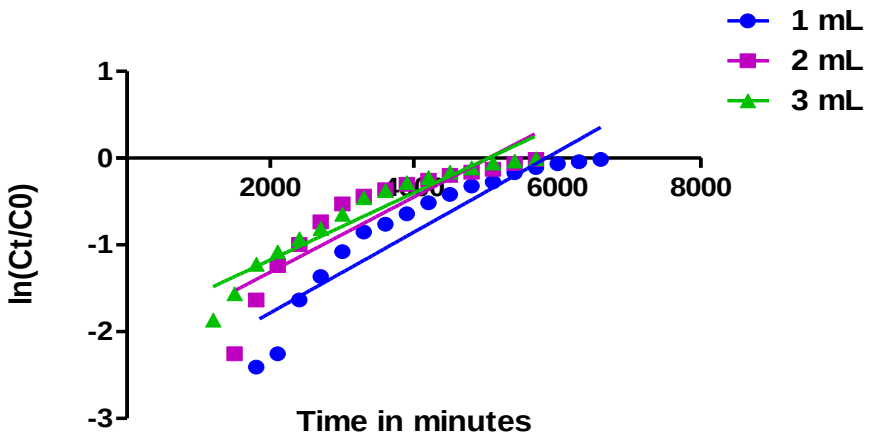

Figure 19: Effect of flow rate: Adam Bohart kinetic plot for the adsorption of Lead onto CMC-HAp-f-GO-GLU composite

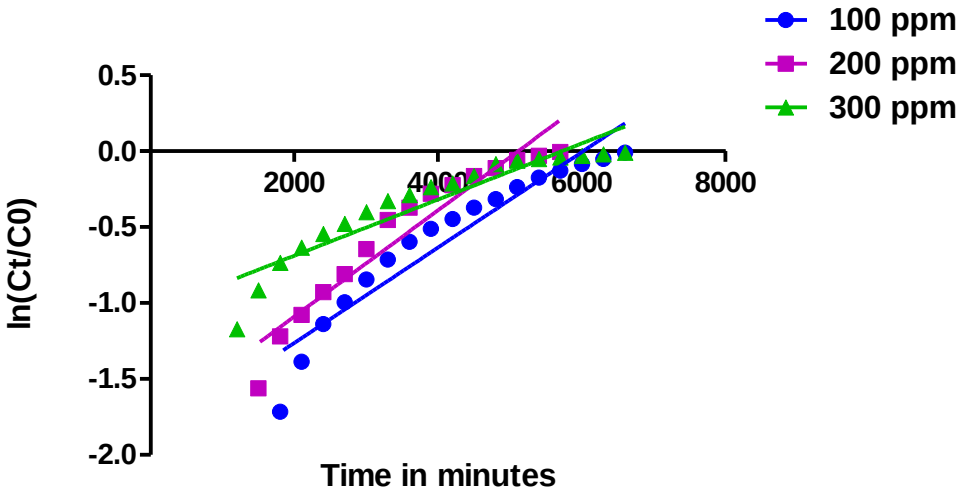

Figure 20: Effect of initial metal ion concentration: Adam Bohart kinetic plot for the adsorption of Lead onto CMC-HAp-f-GO-GLU composite

Table 7
Adam Bohart model parameters at different conditions using linear regression analysis for the adsorption of Lead (II) onto CMC-HAp-f-GO-GLU composite

Flow rate (mL/ min)	Bed height (cm)	Inlet conc (mg/ L)	Constant		
			kAB (mL/min.mg) (x 10^{-6})	No (mg/L) ($X10^4$)	R^2
1.0	1.0	200	2.321	13.28	0.8659
2.0	1.0	200	2.159	22.92	0.7989
3.0	1.0	200	1.930	34.38	0.9108
3.0	1.0	**100**	3.143	20.54	0.9104
3.0	1.0	**200**	1.930	34.38	0.9108
3.0	1.0	**300**	1.616	58.61	0.8696

From figures 19 and 20, it is clear that when the initial metal ion concentration and the flow rate increased, so did the N_o. This can be explained by the fact that more adsorbate molecules pass through the adsorbent at high flow rates, which raises the rate. Okewale et al[56] suggested that as the flow rate of the metal ion solution increased, the N_o value also increased.

Thomas Model: One of the most popular models for interpreting results from fixed-bed column adsorption is the Thomas equation. According to this model, the adsorption process data adheres to the Langmuir isotherm and second-order reversible reaction kinetics. It is assumed that there is no internal or external dispersion restriction[15]. Additionally, the linearized form of the Thomas model for an adsorption

column was expressed as follows. The data obtained from the adsorption process conforms to the second-order reversible reaction kinetics and the Langmuir isotherm.

$$\ln\left(\frac{C_0}{C_t}-1\right)=\frac{K_{TH}q_0X}{Q}-\frac{K_{TH}C_0}{Q}V_{eff}$$

where V_{eff} is the throughput volume (mL), X is the total mass of the adsorbent (g), Q is the inlet volumetric flow rate (ml/min), q_o is the maximal adsorption capacity (mg/g) and k_{TH} is the Thomas rate constant (mL/min.mg). By applying linear regression to plot ln (C_o/C_t-1) versus throughput volume (V_{eff}), the k_{TH} and q_o can be found from the slope and intercept of the graph.

Figures 21 and 22 represent the Thomas model's linear plot using experimental data at starting metal ion concentrations (100 mg/L to 300 mg/L), flow rates (1 mL/min to 3 mL/min) and bed height (1 cm) for Pb (II) onto CMC-HAp-f-GO-GLU composite. Table 8 represents the Thomas model parameters and R^2 computed using linear regression analysis under different conditions for the CMC-HAp-f-GO-GLU composite. The flow rate, initial ion concentration and bed height all had an impact on the Thomas rate constant, or k_{TH}, according to the table's data. k_{TH} characterizes the speed of metal ion transport from solution to adsorbent. The maximal adsorption capacity, or q_o, grew in proportion to the original metal ion concentration and flow rate

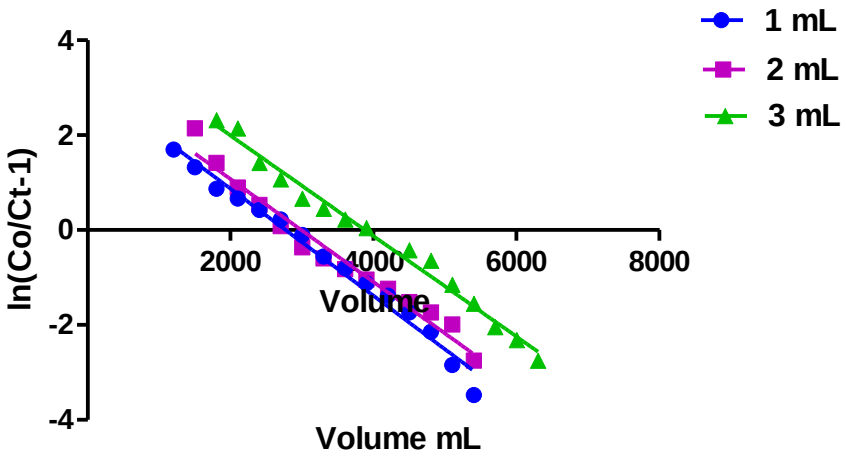

Figure 21: Effect of flow rate: Thomas kinetic plot for the adsorption of Lead onto CMC-HAp-f-GO-GLU composite

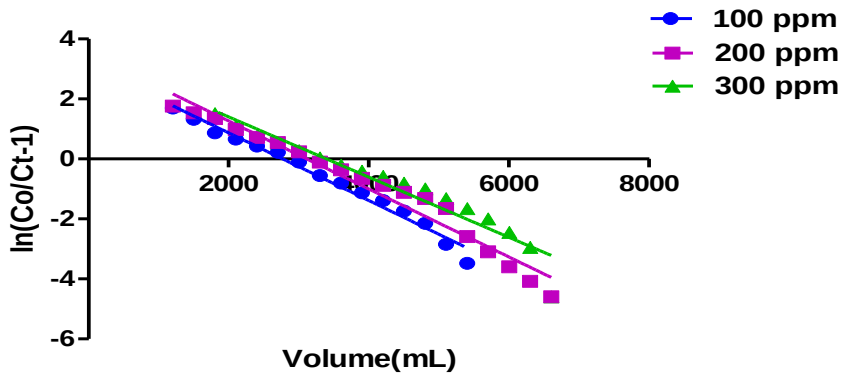

Figure 22: Effect of initial metal ion concentration: Thomas kinetic plot for the adsorption of Lead onto CMC-HAp-f-GO-GLU composite

Table 8
Thomas model parameters at different conditions using linear regression analysis for the adsorption of Lead (II) onto CMC-HAp-f-GO-GLU composite

Flow rate (mL/ min)	Bed height (cm)	Inlet conc (mg/ L)	Constant		
			k_{TH} (mL/ min. mg) ($\times 10^{-6}$)	q_0 (mg/g) ($\times 10^4$)	R^2
1.0	1.0	200	5.3	17.5	0.9861
2.0	1.0	200	10.84	25.9	0.9691
3.0	1.0	200	16.9	55.4	0.9819
3.0	1.0	**100**	17.8	52.6	0.9298
3.0	1.0	**200**	16.9	55.4	0.9819
3.0	1.0	**300**	11.33	93.44	0.9674

Correlation coefficient (R^2) was determined for the Thomas model under various operating conditions. It was found to be more than 0.9, indicating a good confirmation and perfect fit of the kinetic data into the model. Therefore, it is possible to suggest that the Thomas model could explain the column's total adsorption kinetics.

Yoon Nelson model: According to the Yoon-Nelson model, each solute molecule's rate of decrease in sorption probability is considered to be proportionate to molecule's probability of sorption and the breakthrough of the adsorbate on the adsorbent[54]. For a system with just one component, the linearized model is expressed as:

$$\ln\left(\frac{Ct}{Co-Ct}\right) = K_{YN}t - K_{YN}\,\tau$$

where the concentrations of intake and effluent solutes are represented by the variables C_t and C_o, k_{YN} is the Yoon and Nelson rate constant (min^{-1}), t is the breakthrough (sampling) time (min) and τ is the time required for 50% adsorbate breakthrough (min). A straight line with an intercept of $-\tau\ k_{YN}$ and a slope of k_{YN} is obtained when plotting $\ln (C_t/C_o-C_t)$ against t. The k_{YN} and τ values were computed using the slope and intercept of the figure shown (Figures 23 and 24). Figures 23 and 24 and table 9 depict the Yoon Nelson model parameters' computed values and the correlation coefficients using linear regression analysis in different situations for CMC-HAp-f-GO-GLU composite on Pb (II) adsorption.

According to the data, the metal ion concentration and flow rate increased with a constant bed height, causing the K_{YN} to rise. The high values of the regression coefficient that were found, indicate that the Yoon and Nelson model fits the experimental data rather well. The duration needed for 50% breakthrough, τ, reduced as concentrations of metal ions and flow rate both rose[32]. The rapid attainment of column saturation may be the cause of the fall in τ value. Because of the slower saturation at higher bed heights, this will be the opposite in the case of bed height[71]. Eventually, tables 7 to 9 indicate that the correlation coefficients range from 0.8903 to 0.9819. indicating that the kinetic data of the Thomas model and Yoon-Nelson are better fitted to this model.

The correlation coefficients (R^2) of the Thomas and Yoon-Nelson models in a fixed bed column that are listed in tables 8 and 9 offer the best fit ($R^2 > 0.9$) to the experimental data under different conditions[2].

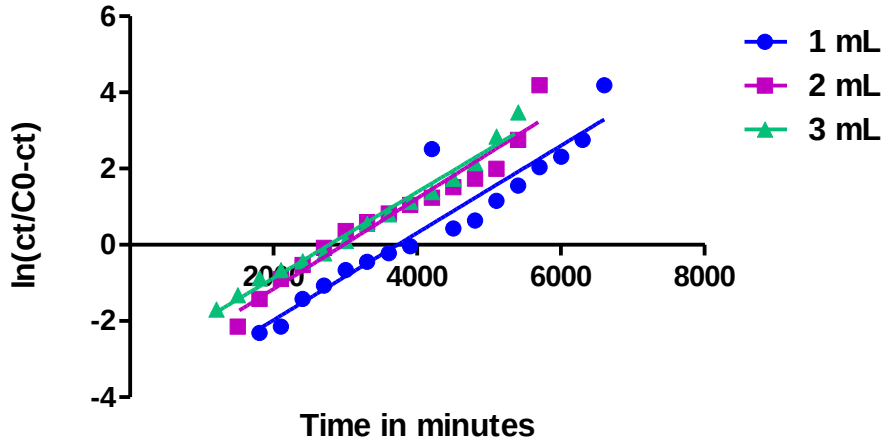

Figure 23: Effect of flow rate: Yoon Nelson kinetic plot for the adsorption of Lead onto CMC-HAp-f-GO-GLU composite

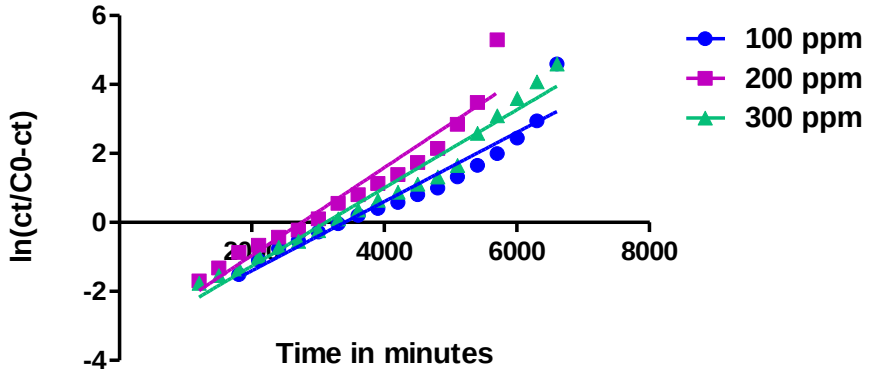

Figure 24: Effect of initial metal ion concentration: Yoon Nelson kinetic plot for the adsorption of Lead onto CMC-HAp-f-GO-GLU composite

Table 9
Yoon Nelson model parameters at different conditions using linear regression analysis for the adsorption of Lead (II) onto CMC-HAp-f-GO-GLU composite

Flow rate (mL/min)	Bed height (cm)	Inlet conc (mg/L)	Constant		
			K_{YN} (min^{-1}) (10^{-3})	τ (min) (10^3)	R^2
1.0	1.0	200	1.044	3.724	0.8903
2.0	1.0	200	1.088	2.973	0.9482
3.0	1.0	200	1.127	2.771	0.9819
3.0	1.0	**100**	1.004	3.394	0.9298
3.0	1.0	**200**	1.127	2.771	0.9316
3.0	1.0	**300**	1.133	2.114	0.9674

It is thus confirmed that a column with an adsorbent of 1cm bed height, a flow rate of 3 ml/min and a concentration of Lead solution with 200 mg/L are the ideal conditions for effective remediation of heavy metal lead from aqueous solution. Hence, the Thomas and Yoon-Nelson models can be used to study the adsorption of lead on the CMC/HAp/f-GO-GLU composite.

Conclusion

f-GO-based glutaraldehyde cross-linked composite constitutedof carboxymethyl cellulose and hydroxyapatite (CMC/HAp/f-GO-GLU) was prepared and characterized using FT-IR, XRD, TGA, DSC, SEM, antimicrobial and antioxidant studies. The results of the characterization techniques revealed the good miscibility of thecomponents in the polymer matrix. The higher thermal stability, rough surface morphology and high surface area of the composite established the good adsorbent capacity through the investigation of the removal of lead and mercury heavy metals removal by optimizing the dosage of the adsorbent, pH, duration of contact and starting metal ion concentration.

The sorption capacity of the adsorbent is strongly dependent on these factors. The kinetic studies demonstrated that the equilibrium data fit the Freundlich model better than the Langmuir isotherm model and the adsorbent followed pseudo-second-order. The adsorption of the metal ions onto the adsorbent was proved by taking the FT-IR and EDX analysis of the metal-loaded sample. The column study's findings showed that a starting metal ion concentration of 200 mg/L and an optimal flow rate of 3 ml/min are required. The adsorbent capacity through column study was studied by the breakthrough curves obtained for various models predicted there.

Based on the R^2 value, the Thomas model and Yoon-Nelson model can explain well about the adsorption capacity through the column better than the Adam-Bohart model, with a well fit of experimental values. Hence, the overall results revealed that the prepared glutaraldehyde crosslinked (CMC/HAp/f-GO-GLU) composite demonstrated its effectiveness as an adsorbent with a higher percentage of removal capacity that is appropriate for the adsorption of lead metal. Hence, it can be concluded that the prepared CMC/HAp/f-GO-GLU composite crosslinked with glutaraldehyde crosslinker showed promise as an adsorbent for removing heavy metals from wastewater.

References

1. Agarwal S. et al, Efficient removal of toxic bromothymol blue and methylene blue from wastewater by polyvinyl alcohol, *Journal of Molecular Liquids*, **218**, 191–197 **(2016)**

2. Ahmad A.A. and Hameed B.H., Fixed-bed adsorption of reactive azo dye onto granular activated carbon prepared from waste, *Journal of Hazardous Materials*, **175(1-3)**, 298–303 **(2010)**

3. Ajitha P., Vijayalakshmi K., Saranya M., Gomathi T., Rani K., Sudha P.N. and Sukumaran A., Removal of toxic heavy metal lead (II) using chitosan oligosaccharide-graft-maleic anhydride/ polyvinyl alcohol/silk fibroin composite, *International Journal of Biological Macromolecules*, **104**, 1469–1482 **(2017)**

4. Akhavan O. and Ghaderi E., Toxicity of graphene and graphene oxide nanowalls against bacteria, *ACS Nano*, **4(10)**, 5731–5736 **(2010)**

5. Aksu Z., Çağatay S.S. and Gönen F., Continuous fixed-bed biosorption of reactive dyes by dried *Rhizopus arrhizus*: determination of column capacity, *Journal of Hazardous Materials*, **143(1-2)**, 362–371 **(2007)**

6. Alharbi O.M., Khattab R.A. and Ali I., Health and environmental effects of persistent organic pollutants, *Journal of Molecular Liquids*, **263**, 442–453 **(2018)**

7. Al-Husseiny H.A., Adsorption of methylene blue dye using low cost adsorbent of sawdust: batch and continuous studies, *Journal of Babylon University/Engineering Sciences*, **22(2)**, 296–310 **(2014)**

8. AL Zaher Razan M., Abderrahman Salim M., Abdulateef Safa M., Dheeb Batol Imran, Massadeh Muhannad I., Hussein Anmar Sael and Farhan Mohammed Sami, Antimicrobial activity of Zn-nanoparticles synthesized by leaf extract of Capparis spinosa, *Res. J. Biotech.*, **19(11)**, 14–21 **(2024)**

9. Amin M.T., Alazba A.A. and Shafiq M., Removal of copper and lead using banana biochar in batch adsorption systems: isotherms and kinetic studies, *Arabian Journal for Science and Engineering*, **43**, 5711–5722 **(2018)**

10. Balarak D. and Mostafapour F.K., Canola residual as a biosorbent for antibiotic metronidazole removal, *The Pharmaceutical and Chemical Journal*, **3(2)**, 12–17 **(2016)**

11. Bao Y., Ma J. and Li N., Synthesis and swelling behaviors of sodium carboxymethyl cellulose-g-poly(AA-co-AM-co-AMPS)/ MMT superabsorbent hydrogel, *Carbohydrate Polymers*, **84(1)**, 76–82 **(2011)**

12. Bohart G.S. and Adams E.Q., Some aspects of the behavior of charcoal with respect to chlorine, *Journal of the American Chemical Society*, **42(3)**, 523–544 **(1920)**

13. Chen J., Liao C., Guo X.X., Hou S.C. and He W.D., PAAO cryogels from amidoximated P(acrylic acid-co-acrylonitrile) for the adsorption of lead ion, *European Polymer Journal*, **171**, 111192 **(2022)**

14. Chen L., Ramadan A., Lü L., Shao W., Luo F. and Chen J., Biosorption of methylene blue from aqueous solution using lawny grass modified with citric acid, *Journal of Chemical & Engineering Data*, **56(8)**, 3392–3399 **(2011)**

15. Chen S., Yue Q., Gao B., Li Q., Xu X. and Fu K., Adsorption of hexavalent chromium from aqueous solution by modified corn stalk: a fixed-bed column study, *Bioresource Technology*, **113**, 114–120 **(2012)**

16. Chen X., Wu Y.T., Wang X. and Ma C.F., Experimental study on thermophysical properties of molten salt nanofluids prepared by high-temperature melting, *Solar Energy Materials and Solar Cells*, **191**, 209–217 **(2019)**

17. Copello G.J., Varela F., Vivot R.M. and Díaz L.E., Immobilized chitosan as biosorbent for the removal of Cd(II), Cr(III) and Cr(VI) from aqueous solutions, *Bioresource Technology*, **99(14)**, 6538–6544 **(2007)**

18. Esmaeili A. and Khoshnevisan N., Optimization of process parameters for removal of heavy metals by biomass of Cu and Co-doped alginate-coated chitosan nanoparticles, *Bioresource Technology*, **218**, 650–658 **(2016)**

19. Fahrurrozi M. and Wirawan S.K., Antioxidant activity and controlled release analysis of red ginger oleoresin (*Zingiber officinale var rubrum*) encapsulated in chitosan cross-linked by glutaraldehyde saturated toluene, *Sustainable Chemistry and Pharmacy*, **12**, 100132 **(2019)**

20. Foroutan R., Peighambardoust S.J., Ahmadi A., Akbari A., Farjadfard S. and Ramavandi B., Adsorption of mercury, cobalt and nickel with a reclaimable and magnetic composite of hydroxyapatite/Fe_3O_4/polydopamine, *Journal of Environmental Chemical Engineering*, **9(4)**, 105709 **(2021)**

21. Garai S. and Sinha A., Biomimetic nanocomposites of carboxymethyl cellulose–hydroxyapatite: Novel three dimensional load bearing bone grafts, *Colloids and Surfaces B: Biointerfaces*, **115**, 182–190 **(2014)**

22. Garavand F., Rouhi M., Razavi S.H., Cacciotti I. and Mohammadi R., Improving the integrity of natural biopolymer films used in food packaging by crosslinking approach: A review, *International Journal of Biological Macromolecules*, **104**, 687–707 **(2017)**

23. Gopalakrishnan A., Krishnan R., Thangavel S., Venugopal G. and Kim S.J., Removal of heavy metal ions from pharma-effluents using graphene-oxide nanosorbents and study of their adsorption kinetics, *Journal of Industrial and Engineering Chemistry*, **30**, 14–19 **(2015)**

24. Han M. et al, Phase migration and transformation of uranium in mineralized immobilization by wasted bio-hydroxyapatite, *Journal of Cleaner Production,* **197**, 886–894 **(2018)**

25. Hao L., Lv Y. and Song H., The morphological evolution of hydroxyapatite on high-efficiency Pb^{2+} removal and antibacterial activity, *Microchemical Journal*, **135**, 16–25 **(2017)**

26. He T., Liu S., Lv S., Wei D. and Liu L., Three-dimensional graded porous structure and compressible KGM-GO/CS/SA composite aerogel spheres for efficient adsorption of antibiotics, *Separation and Purification Technology*, **346**, 127547 **(2024)**

27. Hokkanen S., Bhatnagar A. and Sillanpää M., A review on modification methods to cellulose-based adsorbents to improve adsorption capacity, *Water Research*, **91**, 156–173 **(2016)**

28. Hu H., Chang M., Zhang M., Wang X. and Chen D., A new insight into PAM/graphene-based adsorption of water-soluble aromatic pollutants, *Journal of Materials Science*, **52(14)**, 8650–8664 **(2017)**

29. Hu N. et al, A facile route for the large scale fabrication of graphene oxide papers and their mechanical enhancement by cross-linking with glutaraldehyde, *Nano-Micro Letters*, **3**, 215–222 **(2011)**

30. Jung K.W. et al, A facile one-pot hydrothermal synthesis of hydroxyapatite/biochar nanocomposites: adsorption behavior and mechanisms for the removal of copper(II) from aqueous media, *Chemical Engineering Journal*, **369**, 529–541 **(2019)**

31. Kamarudin K.H. and Isa M.I.N., Structural and DC Ionic conductivity studies of carboxymethyl cellulose doped with ammonium nitrate as solid polymer electrolytes, *International Journal of Physical Sciences*, **8(31)**, 1581–1587 **(2013)**

32. Khatibikamal V., Torabian A. and Baghdadi M., Stabilizing of poly (amidoamine) dendrimer on the surface of sand for the removal of nonylphenol from water: batch and column studies, *Journal of Hazardous Materials*, **367**, 357–364 **(2019)**

33. Kim S.S., Park M.S., Jeon O., Choi C.Y. and Kim B.S., Poly (lactide-co-glycolide)/hydroxyapatite composite scaffolds for bone tissue engineering, *Biomaterials*, **27(8)**, 1399–1409 **(2006)**

34. Krumova M., Lopez D., Benavente R., Mijangos C. and Perena J.M., Effect of crosslinking on the mechanical and thermal properties of poly (vinyl alcohol), *Polymer*, **41(26)**, 9265–9272 **(2000)**

35. Kulkarni P.S., Deshmukh P.G., Jakhade A.P., Kulkarni S.D. and Chikate R.C., 1,5-Diphenyl carbazide immobilized cross-linked chitosan films: An integrated approach towards enhanced removal of Cr(VI), *Journal of Molecular Liquids*, **247**, 254–261 **(2017)**

36. Kyzas G.Z. et al, Graphene oxide and its application as an adsorbent for wastewater treatment, *Journal of Chemical Technology & Biotechnology*, **89(2)**, 196–205 **(2014)**

37. Lavanya R., Gomathi T., Nithya R. and Sudha P.N., Fixed-bed column adsorption studies of lead (II) from aqueous solution using chitosan-g-maleic anhydride-g-methacrylic acid copolymer, *Journal of Science and Technology*, **5(4)**, 3163-334 **(2020)**

38. Lavanya R., Gomathi T., Vijayalakshmi K., Saranya M., Sudha P.N. and Anil S., Adsorptive removal of copper (II) and lead (II) using chitosan-g-maleic anhydride-g-methacrylic acid copolymer, *International Journal of Biological Macromolecules*, **104**, 1495–1508 **(2017)**

39. Lehmann M., Zouboulis A.I. and Matis K.A., Modelling the sorption of metals from aqueous solutions on goethite fixed-beds, *Environmental Pollution*, **113(2)**, 121–128 **(2001)**

40. Li W., Dobraszczyk B.J., Dias A. and Gil A.M., Polymer conformation structure of wheat proteins and gluten subfractions revealed by ATR-FTIR, *Cereal Chemistry,* **83(4)**, 407–410 **(2006)**

41. Lin S. et al, Environmental lead pollution and elevated blood lead levels among children in a rural area of China, *American Journal of Public Health*, **101(5)**, 834–841 **(2011)**

42. Liu M. et al, Design of bionic amphoteric adsorbent based on reed root loaded with amino-functionalized magnetic nanoparticles for heavy metal ions removal, *Industrial Crops and Products*, **188**, 115591 **(2022)**

43. Liu S. et al, Antibacterial activity of graphite, graphite oxide, graphene oxide and reduced graphene oxide: membrane and oxidative stress, *ACS Nano*, **5(9)**, 6971–6980 **(2011)**

44. Liu Y., Li M. and He C., Removal of Cr(VI) and Hg(II) ions from wastewater by novel β-CD/MGO-SO_3H composite, *Colloids and Surfaces A: Physicochemical and Engineering Aspects*, **512**, 129–136 **(2017)**

45. Liu Y., Luo D. and Wang T., Hierarchical structures of bone and bioinspired bone tissue engineering, *Small*, **12(34)**, 4611–4632 **(2016)**

46. Ma M.G. et al, Rapid microwave-assisted synthesis and characterization of cellulose-hydroxyapatite nanocomposites in N, N-dimethylacetamide solvent, *Carbohydrate Research*, **345(8)**, 1046–1050 **(2010)**

47. Makeswari M., Santhi T. and Aswini P.K., Adsorption of nickel ions by using binary metal oxides from aqueous solution, *International Journal of Advanced Research*, **4(2)**, 542–553 **(2016)**

48. Mane S., Ponrathnam S. and Chavan N., Effect of chemical cross-linking on properties of polymer microbeads: A review, *Canadian Chemical Transactions*, **3(4)**, 473–485 **(2015)**

49. Matinfar M., Mesgar A.S. and Mohammadi Z., Evaluation of physicochemical, mechanical and biological properties of chitosan/carboxymethyl cellulose reinforced with multiphasic calcium phosphate whisker-like fibers for bone tissue engineering, *Materials Science and Engineering: C*, **100**, 341–353 **(2019)**

50. Miljković V., Gajić I. and Nikolić L., Waste materials as a resource for production of CMC superabsorbent hydrogel for sustainable agriculture, *Polymers*, **13(23)**, 4115 **(2021)**

51. Miretzky P. and Cirelli A.F., Hg(II) removal from water by chitosan and chitosan derivatives: a review, *Journal of Hazardous Materials*, **167(1–3)**, 10–23 **(2009)**

52. Mocanu A. et al, Synthesis, characterization and antimicrobial effects of composites based on multi-substituted hydroxyapatite and silver nanoparticles, *Applied Surface Science*, **298**, 225–235 **(2014)**

53. Mohamed M.A., Jaafar J., Ismail A.F., Othman M.H.D. and Rahman M.A., Fourier transform infrared (FTIR) spectroscopy, *Membrane Characterization*, 3–29, DOI:10.1016/B978-0-444-63776-5.00001-2 **(2017)**

54. Mohammad Y.S., Shaibu-Imodagbe E.M., Igboro S.B., Giwa A. and Okuofu C.A., Adsorption of phenol from refinery wastewater using rice husk activated carbon, *Iranica Journal of Energy & Environment*, **5(4)**, DOI:10.5829/idosi.ijee.2014.05.04.07 **(2014)**

55. Mudipalli A., Lead hepatotoxicity & potential health effects, *Indian Journal of Medical Research*, **126(6)**, 518–527 **(2007)**

56. Okewale A.O., Igbokwe P.K. and Babayemi K.A., Design of pilot plant packed column for the dehydration of water from ethanol-water mixtures, *Advances in Chemical Engineering and Science*, **5(2)**, 152 **(2015)**

57. Pandey L.M., Surface engineering of nano-sorbents for the removal of heavy metals: Interfacial aspects, *Journal of Environmental Chemical Engineering*, **9(1)**, 104586 **(2021)**

58. Panwar V., Chattree A. and Pal K., A new facile route for synthesizing of graphene oxide using mixture of sulfuric–nitric–phosphoric acids as intercalating agent, *Physica E: Low-dimensional Systems and Nanostructures*, **73**, 235–241 **(2015)**

59. Patel H., Fixed-bed column adsorption study: a comprehensive review, *Applied Water Science*, **9(3)**, 45 **(2019)**

60. Peng X., Yan J., He C., Liu R. and Liu Y., Sustainable triethylenetetramine modified sulfonated graphene oxide/chitosan composite for enhanced adsorption of Pb(II), Cd(II) and Ni(II) ions, *International Journal of Biological Macromolecules*, **261**, 129741 **(2024)**

61. Prasad P.S., Gomathi T., Sudha P.N., Deepa M., Rambabu K. and Banat F., Biosilica/Silk Fibroin/Polyurethane biocomposite for toxic heavy metals removal from aqueous streams, *Environmental Technology & Innovation*, **28**, 102741, DOI: 10.1016/j.eti.2022.102741 **(2022)**

62. Qi X., Tong X., Pan W., Zeng Q., You S. and Shen J., Recent advances in polysaccharide-based adsorbents for wastewater treatment, *Journal of Cleaner Production*, **315**, 128221 **(2021)**

63. Queiroz M.F., Teodosio Melo K.R., Sabry D.A., Sassaki G.L. and Rocha H.A.O., Does the use of chitosan contribute to oxalate kidney stone formation?, *Marine Drugs*, **13(1)**, 141–158 **(2014)**

64. Rajesh A., Mangamma G., Sairam T.N., Subramanian S., Kalavathi S., Kamruddin M. and Dash S., Physicochemical properties of nanocomposite: Hydroxyapatite in reduced graphene oxide, *Materials Science and Engineering: C*, **76**, 203–210 **(2017)**

65. Rajeswari A., Amalraj A. and Pius A., Adsorption studies for the removal of nitrate using chitosan/PEG and chitosan/PVA polymer composites, *Journal of Water Process Engineering*, **9**, 123–134 **(2016)**

66. Rani K., Gomathi T., Vijayalakshmi K., Saranya M. and Sudha P.N., Banana fiber cellulose nanocrystals grafted with butyl acrylate for heavy metal lead (II) removal, *International Journal of Biological Macromolecules*, **131**, 461–472 **(2019)**

67. Rasoulzadeh M. and Namazi H., Carboxymethyl cellulose/graphene oxide bio-nanocomposite hydrogel beads as anticancer drug carrier agent, *Carbohydrate Polymers*, **168**, 320–326 **(2017)**

68. Rekha A. et al, Biosorption efficacy studies of Sargassum wightii and its biochar on the removal of chromium from aqueous solution, *Journal of the Taiwan Institute of Chemical Engineers*, 105241, DOI: 10.1016/j.jtice.2023.105241 **(2023)**

69. Rekha A., Vijayalakshmi K., Alswieleh A., Sudha P.N., Rani J. and Vidhya A., Enhanced removal of Cr(VI) from water using alginate-modified algal biochar: a promising adsorbent, *Biomass Conversion and Biorefinery*, DOI:10.1007/s13399-024-05792-y **(2024)**

70. Robati D., Mirza B., Rajabi M., Moradi O., Tyagi I., Agarwal S. and Gupta V.K., Removal of hazardous dyes-BR 12 and methyl orange using graphene oxide as an adsorbent from aqueous phase, *Chemical Engineering Journal*, **284**, 687–697 **(2016)**

71. Saadi Z., Saadi R. and Fazaeli R., Fixed-bed adsorption dynamics of Pb (II) adsorption from aqueous solution using nanostructured γ-alumina, *Journal of Nanostructure in Chemistry*, **3,** 1–8 **(2013)**

72. Saito Y., Okada K., Endo T. and Sakakibara K., Highly surface-selective nitration of cellulose nanofibers under mildly acidic reaction conditions, *Cellulose*, **30(16)**, 10083–10095 **(2023)**

73. Saleh T.A., Nanocomposite of carbon nanotubes/silica nanoparticles and their use for adsorption of Pb(II): from surface properties to sorption mechanism, *Desalination and Water Treatment*, **57(23)**, 10730–10744 **(2016)**

74. Sathiyanarayanan P. and Karunakaran R.J., Batch adsorptive removal of copper (II) using carboxymethyl cellulose (CMC), polyethylene glycol (PEG) and montmorillonite (MMT) clay ternary blend, *Journal of Chemical and Pharmaceutical Research,* **7(4)**, 1099–1108 **(2015)**

75. Shah H.U.R., Ahmad K., Naseem H.A., Parveen S., Ashfaq M., Rauf A. and Aziz T., Water stable graphene oxide metal-organic frameworks composite (ZIF-67@GO) for efficient removal of malachite green from water, *Food and Chemical Toxicology*, **154**, 112312 **(2021)**

76. Shi Y.Y., Li M., Liu Q., Jia Z.J., Xu X.C., Cheng Y. and Zheng Y.F., Electrophoretic deposition of graphene oxide reinforced chitosan–hydroxyapatite nanocomposite coatings on Ti substrate, *Journal of Materials Science: Materials in Medicine*, **27**, 1–13 **(2016)**

77. Singh P., Medronho B., Alves I., Da Silva G.J., Miguel M.G. and Lindman B., Development of carboxymethyl cellulose-chitosan hybrid micro-and macroparticles for encapsulation of probiotic bacteria, *Carbohydrate Polymers*, **175**, 87–95 **(2017)**

78. Srinivasan A. and Viraraghavan T., Decolorization of dye wastewaters by biosorbents: a review, *Journal of Environmental Management*, **91(10)**, 1915–1929 **(2010)**

79. Stankovich S. et al, Synthesis of graphene-based nanosheets via chemical reduction of exfoliated graphite oxide, *Carbon*, **45(7)**, 1558–1565 **(2007)**

80. Su Y., Wang J., Li S., Zhu J., Liu W. and Zhang Z., Self-templated microwave-assisted hydrothermal synthesis of two-dimensional holey hydroxyapatite nanosheets for efficient heavy metal removal, *Environmental Science and Pollution Research,* **26**, 30076–30086 **(2019)**

81. Syama S. and Mohanan P.V., Comprehensive application of graphene: emphasis on biomedical concerns, *Nano-Micro Letters*, **11**, 1–31 **(2019)**

82. Szostak K., Hodacka G., Długosz O., Pulit-Prociak J. and Banach M., Sorption of mercury in batch and fixed-bed column system on hydrochar obtained from apple pomace, *Processes*, **10(10)**, 2114 **(2022)**

83. Taty-Costodes V.C., Fauduet H., Porte C. and Ho Y.S., Removal of lead (II) ions from synthetic and real effluents using immobilized *Pinus sylvestris* sawdust: adsorption on a fixed-bed column, *Journal of Hazardous Materials*, **123(1-3)**, 135–144 **(2005)**

84. Tel H., Altaş Y. and Taner M.S., Adsorption characteristics and separation of Cr(III) and Cr(VI) on hydrous titanium(IV) oxide, *Journal of Hazardous Materials*, **112(3)**, 225–231 **(2004)**

85. Tofighy M.A. and Mohammadi T., Copper ions removal from aqueous solutions using acid-chitosan functionalized carbon nanotubes sheets, *Desalination and Water Treatment*, **57(33)**, 15384–15396 **(2016)**

86. Waheed A., Baig N., Ullah N. and Falath W., Removal of hazardous dyes, toxic metal ions and organic pollutants from wastewater by using porous hyper-cross-linked polymeric materials: A review of recent advances, *Journal of Environmental Management*, **287**, 112360 **(2021)**

87. Wakeland S., Martinez R., Grey J.K. and Luhrs C.C., Production of graphene from graphite oxide using urea as expansion–reduction agent, *Carbon*, **48(12)**, 3463–3470 **(2010)**

88. Wang D., Liu L., Jiang X., Yu J. and Chen X., Adsorption and removal of malachite green from aqueous solution using magnetic β-cyclodextrin-graphene oxide nanocomposites as adsorbents, *Colloids and Surfaces A: Physicochemical and Engineering Aspects*, **466**, 166–173 **(2015)**

89. Wang S. et al, Adsorption of phosphorus by calcium-flour biochar: Isotherm, kinetic and transformation studies, *Chemosphere*, **195**, 666–672 **(2018)**

90. Watwe V. and Kulkarni P., Evaluation of Cr(VI) adsorption on glutaraldehyde crosslinked chitosan beads using cyclic voltammetry employing gold electrode, *Journal of Analytical Science and Technology*, **12**, 1–10 **(2021)**

91. Wei M.P., Chai H., Cao Y.L. and Jia D.Z., Sulfonated graphene oxide as an adsorbent for removal of Pb^{2+} and methylene blue, *Journal of Colloid and Interface Science*, **524**, 297–305 **(2018)**

92. Yadav M., Rhee K.Y., Jung I.H. and Park S.J., Eco-friendly synthesis, characterization and properties of a sodium carboxymethyl cellulose/graphene oxide nanocomposite film, *Cellulose*, **20**, 687–698 **(2013)**

93. Yadav S.K., Yoo H.J. and Cho J.W., Click coupled graphene for fabrication of high-performance polymer nanocomposites, *Journal of Polymer Science Part B: Polymer Physics*, **51(1)**, 39–47 **(2013)**

94. Yu S. et al, One-pot synthesis of graphene oxide and Ni-Al layered double hydroxides nanocomposites for the efficient removal of U (VI) from wastewater, *Science China Chemistry*, **60**, 415–422 **(2017)**

95. Yu W., Sisi L., Haiyan Y. and Jie L., Progress in the functional modification of graphene/graphene oxide: A review, *RSC Advances*, **10(26)**, 15328–15345 **(2020)**

96. Zaynab M., Al-Yahyai R., Ameen A., Sharif Y., Ali L., Fatima M. and Li S., Health and environmental effects of heavy metals, *J King Saud Univ Sci*., **34(1)**, 101653 **(2022)**

97. Zhang L., Luo H., Liu P., Fang W. and Geng J., A novel modified graphene oxide/chitosan composite used as an adsorbent for Cr (VI) in aqueous solutions, *International Journal of Biological Macromolecules*, **87**, 586–596 **(2016)**

98. Zhang X. et al, Distribution and biocompatibility studies of graphene oxide in mice after intravenous administration, *Carbon,* **49(3)**, 986–995 **(2011)**

99. Zhang Y., Zhong C., Zhang Q., Chen B., He M. and Hu B., Graphene oxide–TiO_2 composite as a novel adsorbent for the preconcentration of heavy metals and rare earth elements in environmental samples followed by online inductively coupled plasma optical emission spectrometry detection, *RSC Advances*, **5(8)**, 5996–6005 **(2015)**

100. Zhao G., Jiang L., He Y., Li J., Dong H., Wang X. and Hu W., Sulfonated graphene for persistent aromatic pollutant management, *Advanced Materials*, **23(34)**, 3959–3963 **(2011)**

101. Zhao G., Li J., Ren X., Chen C. and Wang X., Few-layered graphene oxide nanosheets as superior sorbents for heavy metal ion pollution management, *Environmental Science & Technology*, **45(24)**, 10454–10462 **(2011)**

102. Zhou D., Zhang I., Zhou J. and Guo S., Development of a fixed-bed column with cellulose/chitin beads to remove heavy metal ions, *Journal of Applied Polymer Science*, **94(2),** 684–691 **(2004)**.

(Received 11th June 2025, accepted 08th July 2025)